STUDY OF TRANSITIONS IN A TURBULENT COMBUSTOR USING RECURRENCE NETWORKS

A Project Report

submitted by

VEDASRI GODAVARTHI

in partial fulfilment of the requirements
for the award of the degree of

BACHELOR OF TECHNOLOGY and **MASTER OF TECHNOLOGY**

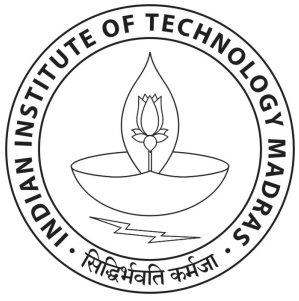

DEPARTMENT OF AEROSPACE ENGINEERING
INDIAN INSTITUTE OF TECHNOLOGY MADRAS

MAY 2019

CERTIFICATE

This is to certify that the project report titled **STUDY OF TRANSITIONS IN A TURBULENT COMBUSTOR USING RECURRENCE NETWORKS**, submitted by **Vedasri Godavarthi**, to the Indian Institute of Technology, Madras, for the award of the degree of **Bacherlor of Technology** and **Masters of Technology**, is a bona fide record of the research work done by her under our supervision. The contents of this thesis, in full or in parts, have not been submitted to any other Institute or University for the award of any degree or diploma.

Prof. R. I. Sujith
Research Guide
Professor
Dept. of Aerospace Engineering
IIT-Madras, 600 036

Place: Chennai

Date: 3rd May 2019

ACKNOWLEDGEMENTS

First and foremost, I am extremely grateful to my project guide, Prof. R. I. Sujith for his continuous support and guidance. His passion for exploring new avenues and perceiving the problem in different ways is extremely inspiring. His enthusiam for research motivates me to work hard and push myself. Working with him has been a delighful experience and also motivated me to pursue research as my career.

I would like to thank the current and the past Heads of the Aerospace Engineering department, Prof. P. Sriram and Prof. K. Bhaskar for their support throughout the past five years. I would also like to thank my professors, Prof. M. Ramakrishna, Prof. Luoyi Tao, Prof. Ranjith Mohan, Prof. Shantanu Ghosh, Prof. A. Sameen, Prof. H. S. N. Murthy from Aerospace Department, Prof. Arun Tangirala (Chemical Engineering) for their in-class and outside of class support.

I would like to acknowledge the funding for my project work from ONRG. I also acknowledge the financial assistance from DST-DAAD which allowed me to meet Dr. N. Marwan and Prof. J. Kurths in PIK, Germany, who helped me in understanding the nuances of recurrence networks. I am grateful to Prof. G. Ambika, Prof. K. P. Harikrishnan and Prof. R. Misra for the discussions on recurrence analysis I had with them.

Next, I would like to sincerely thank Dr. V. R. Unni, Dr. S. A. Pawar and Dr. E. A. Gopalakrishnan for their help in paper writing and sharing their outlook on research with me. They were extremely patient with me and my numerous technical and non-technical questions and doubts. I am also thankful to my lab mates Indu, Abin, Praveen, Sirishendu, Krishna, Amitesh, Alan for reviewing my bad drafts and making them better. I also thank my buddy Rao for sticking with me through thick and thin.

Finally, I should acknowledge my family members, my parents, sister and uncle who always encouraged and supported me in all my decisions. I am grateful for my parents for so many sacrifices they made to ensure that I get an excellent education.

ABSTRACT

KEYWORDS: Thermoacoustic instability; Blowout; Complex networks; Recurrence Networks; Turbulent Reactive Flows; Acoustics; Synchronization; Directional Dependence.

Gas turbines are widely used in the aviation and power industries. Gas turbine combustion is a major source of power production but it is accompanied with emission of pollutants. In order to keep the emissions of the hazardous NOx oxides in check, and to meet the stringent emission requirements, clean combustion is needed. Clean combustion is achieved using operating these engines under lean fuel conditions, where the temperature is low, thereby reducing the production of nitrogen oxides. But when operated under fuel lean conditions, the flame is highly susceptible to the perturbations in the flow field. The operation of engines under these conditions is impaired by the occurrence of thermoacoustic instability and flame blowout.

Thermoacoustic instability occurs when there is positive coupling between the acoustic field and the heat release rate. Thermoacoustic instability is composed of high-amplitude, pressure oscillations. These oscillations are detrimental to the engines due to the increase in thermal and mechanical stresses, resulting in loss of billions of dollars. Flame blowout occurs when the flame ceases to exist in the combustor. This can cause a sudden drop in altitude of an airplane and productivity loss in case of land based gas turbines. However, clean combustion cannot be avoided and increase in fuel efficiency is extremely useful. Hence, there is an exigency to study the transition to thermoacoustic instability and blowout.

Traditionally, the transitions in the thermoacoustic systems are analyzed from a reductionist approach which attempts to analyze a complex system in terms of its constituent elements. Recently, multifractal characteristics are found in combustion noise (pressure oscillations during the stable operation zone) and the acoustic oscillations prior to flame blowout. This indicates the presence of inherent complexity in the system, which is due to the nonlinear interaction between the acoustic field, combustion

kinetics and hydrodynamics. The traditional reductionist approach fails to explain this complexity in the thermoacoustic system.

In this study, complex networks are used to study thermoacoustic system, in our case a turbulent combustor. Since recurrence is a fundamental property of any deterministic dynamical system, we construct the recurrence networks from the acoustic time series and the global heat release rate time series acquired from the combustor. Univariate recurrence networks constructed from the acoustic time series capture the transitions to thermoacoustic instability and lean flame blowout. The singularities present in the time series are captured in the power law degree distributions present in the recurrence networks constructed from combustion noise and oscillations prior to flame blowout. The network measures such as characteristic path length, betweenness centrality change well before these transitions and hence can be used as early warning signals to forewarn thermoacoustic instability and lean blowout.

Since thermoacoustic instability is a result of positive coupling between the acoustic field and the turbulent reactive flow, we analyze the coupled behavior during the transition to thermoacoustic instability via intermittency (a state composed of bursts of large amplitude periodic oscillations appearing at irregular intervals amidst aperiodic fluctuations) using synchronization framework. We quantify the synchronization transitions using the measures derived from recurrences in phase space such as probability of recurrence plots, multivariate recurrence plots and networks. The directional dependence between the acoustic field and the turbulent reactive flow field is determined and a possible asymmetric bidirecional coupling between them is discovered with the heat release rate affecting the acoustic field more than vice versa. This paves a way for developing effective control strategies directed towards the unsteady flame to the mitigate thermoacoustic instability.

TABLE OF CONTENTS

LIST OF FIGURES

ABBREVIATIONS

PS	Phase Synchronization
GS	Generalized Synchronization
IPS	Intermittent Phase Synchronization
RP	Recurrence Plot
RQA	Recurrence Quantification Analysis
DET	Determinism
RR	Recurrence Rate
LPG	Liquefied Petroleum Gas
FTF	Flame Transfer Function
CPR	Correlation of Probability of Recurrence
JPR	Joint Probability of Recurrence
CPL	Characteristic Path Length
CRM	Cross Recurrence Matrix
JRM	Joint Recurrence Matrix
RN	Recurrence Network
CRN	Cross Recurrence Network
JRN	Joint Recurrence Network
RQA	Recurrence Quantification Analysis
DET	Determinism
A	Adjacency Matrix
I	Identity Matrix

NOTATION

Upper-case Roman

D	Inner diameter of burner, mm
M	Embedding dimension obtained from false nearest neighbor
$P(k)$	Degree distribution
k	Degree
b_v	Betweenness Centrality
$P(\tau)$	Probability of recurrence
Re	Reynolds number
$R_{i,j}$	Recurrence matrix
$A_{i,j}$	Adjacency matrix
$JRM_{i,j}$	Joint recurrence matrix
$CRM_{i,j}$	Cross recurrence matrix
$I_{i,j}$	Identity matrix
$\mathcal{T}$	Network Transitivity
Q_τ	Transitivity Ratio
$\mathcal{T}_{XY}$	Cross transitivity
X	State vector
X_f	Normalized flame location
X_n	Vector consists of local maximum in the time series

Lower-case Roman

p'	Acoustic pressure, V
$\dot{q}'$	Heat release rate, V
t	Time, s
u'	Acoustic velocity

Greek

ε	Distance threshold of recurrence
ϕ	Equivalence ratio
Θ	Heaviside step function
τ	Time delay
τ_c	Correlation time

Operators

$\|\|.\|\|$	Euclidean norm

CHAPTER 1

Introduction

Gas turbine combustors are widely used in aviation and power generation industries. In fact, energy conversion through the combustion of fossil fuels is an extremely important technology. However, gas turbine combustion produces a lot of pollutants, mainly harmful nitrogen oxides (NOx) that result in acid rain and smog. Reduction of NOx in gas turbine engnines is a major challenge in gas turbine industry. In order to reduce the NOx emissions, which are produced due to the high temperatures in the combustors, gas turbines are operated in fuel-lean conditions. Lean premixed fuel combustion also allows for complete combustion, thereby increasing the fuel efficiency, in addition to decreasing the NOx emissions. But lean fuel conditions cause the flame to be highly sensitive to perturbations (Richards and Janus, 1997) and gas turbine engines operating in fuel lean conditions are susceptible to thermoacoustic instability and lean blowout.

Thermoacoustic instability arises when there is positive feedback between the unsteady heat release rate and the acoustic field in the combustor. Thermoacoustic instability results in self-excited large amplitude pressure oscillations in the combustor. The combustion in these systems occur in a confined environment and the combustion process is inherently unsteady due to the turbulence in the reactive flow field. The acoustic waves originate from the unsteady flame, travel downstream of the combustion chamber, reflect at the boundaries of the confinement and further affect the combustion process forming a feedback loop. Lord Rayleigh 1878 stated that when the combustion response is positively coupled (i.e., in phase) with the acoustic field, acoustic energy is added into the system. This addition of the acoustic energy results in an indefinite increase in the pressure amplitude, when the driving is greater than the losses. The amplitude saturates once the nonlinearities set in, when the energy added is balanced by the losses in the combustion chamber.

The self-sustained large amplitude pressure oscillations in the combustor chamber has detrimental consequences to the structural integrity of the engine. These oscillations cause sudden enhancement in the heat transfer to the walls increasing the mechanical

and thermal stresses which can result in failure of components (McManus *et al.*, 1993; Lieuwen and Neumeier, 2002; Juniper and Sujith, 2018). Hence, it is important to predict and control thermoacoustic instability. Since thermoacoustic instability is a result of complex interaction between the acoustics, combustion and hydrodynamics, understanding thermoacoustic instability is challenging and compelling.

On the other hand, lean blowout is a state where flame ceases to exist in the combustor. In fuel-lean conditions, the combustion temperature is reduced which decreases the flame speed. Also, the flow speeds in fuel lean conditions is higher than the flame speeds making the flame stabilization in a combustor challenging. In order to stabilize the flame in a combustor, variour flame stabilization mechanisms such as bluff body, swirler, V-gutter etc., to name a few are used. These flame holding mechanisms create low velocity regions, to stabilize the flame. However, when equivalence ratio (ϕ), actual fuel-air ratio to the stoichiometric fuel-air ratio, is reduced below a certain value, the flame ceases to exist in the combustor and propagates outside. This state is referred to as lean blowout and the equivalence ratio after which lean blowout occurs is referred to as the lean blowout limit.

Blowout also has detrimental consequences to the engine. In aircrafts, blowout results in the loss of the thrust generated. This might also lead to a sudden drop in the altitude of the aircraft. In case of land-based gas turbine engines, in addition to power loss, blowout causes complete shutdown and requires re-ignition of the engine resulting in productivity loss. Hence, prediction of lean blowout limit and operating away from it is highly important to avoid the losses due to blowout. Further, there is an exigency to investigate and characterize the dynamics underlying the transitions to thermoacoustic instability and blowout in a turbulent combustor to be able to predict these impending instabilities.

Traditionally, several studies attempted to characterize the dynamics during the stable combustion (referred to as combustion noise) and unstable combustion (thermoacoustic instability and lean blowout). They have shown that in many combustors when the equivalence ratio is varied from fuel rich to fuel lean conditions, the transitions happen from combustion noise to thermoacoustic instability and from thermoacoustic instability to lean blowout. However, they focused on contrasting the dynamics observed within each regime but not on the dynamical transition from combustion noise

to thermoacoustic instability and lean blowout which is important in order to develop a precursor. Nair *et al.* 2014 showed that the transition to thermoacoustic instability from combustion noise occurs through intermittency. Kabiraj *et al.* 2012 detected intermittency prior to blowout in a laminar premixed combustion system and reported a rich dynamical behavior during the transition from combustion instability to lean blowout. Unni *et al.* 2015 developed an uniform framework to study the transition from combustion noise to thermoacoustic instability and to lean blowout using multifractal analysis. Using intermittency, several precursors are developed to predict thermoacoustic instability and to lean blowout. A detailed literature survey on precursors in given in the section 1.5.

However, the dynamics in a turbulent combustor is due to the complex interaction between the acoustic field, combustion and the hydrodynamics and hence the thermoacoustic system can be treated as a complex system. The complex system perspective of a turbulent combustor is discussed in the section 1.4. Complex networks are used to study complex systems. Murugesan & Sujith 2015 constructed visibility networks from the acoustic time series to study the transitions in the thermoacoustic system. The present work focuses on analyzing the transition from combustion noise to thermoacoustic instability and blowout via intermittency using recurrence networks because recurrence is a fundamental property of a deterministic dynamical system.

All the above studies focus on the acoustic data alone. But thermoacoustic instability arises due to the interaction between the acoustic field and the unsteady heat release rate in the combustor. Hence it is vital to study the coupled behavior of the pressure fluctuations and the unsteady flame dynamics. Pawar *et al.* 2017 introduced synchronization framework and studied the transition from combustion noise to thermoacoustic instability via intermittency as a synchronization transition from desynchronized aperiodicity to synchronized order through intermittent phase synchronization. However, in their study, the characterization of the transition was mostly qualitative. Characterization of spatiotemporal behavior of the coupled acoustic field and local heat release rate fluctuations in the reaction field during the intermittency route to thermoacoustic instability was performed by Mondal *et al.* 2017. They observed that the transition from combustion noise (phase asynchornous state) to thermoacoustic instability (phase synchronous state) occurs through the formation of a chimera-like state where the phase asynchronous and the phase synchronous regions coexist at the same instant in the re-

action field. More details on the coupled analysis will be provided in the section 1.3.2. The rigorous quantification of these synchronization states is yet to be done. In addition to this, the directional dependence between the acoustic field and the unsteady flame dynamics in a turbulent combustor is yet to be quantified. This will aid in developing effective control mechanisms to mitigate thermoacoustic instability.

The primary objective of this thesis is to analyze the transitions to thermoacoustic instability and blowout in a turbulent combustor using recurrence networks and develop early warning measures to predict impending thermoacoustic instability and blowout. Further, since thermoacoustic instability is a result of interaction between the acoustic field and the unsteady heat release rate, we study the coupled behavior of acoustic field and the unsteady flame dynamics and identify the directional dependence between them.

1.1 Historic overview of thermoacoustic instability

1.1.1 Brief History

The first observation of combustion driven acoustic oscillations dates back to 1777, when Higgins observed a "singing flame" while burning hydrogen gas in a vertical glass tube to produce water (Higgins, 1802). A musical tone was heard when the flame is brought closer to the lower end of the glass tube. Following this, other researchers also noticed an increase in the amplitude of acoutic oscillations when a flame is placed in a glass tube. They identified that the relation between the frequency and the amplitude of the acoustic wave depends on the size of the tube, boundary conditions of the tube and the position of flame inside the tube (Higgins, 1802; Sondhauss, 1850). Rijke used an open-ended glass tube with a metallic gauge at one of the ends. Sound is generated when the metallic gauge is heated with an external flame until its red hot. The intensity of the sound is maximum when the heater location is at quarter length of the tube. Rijke conjectured that the upward convection of air current is the driver of the acoustic oscillations in the tube (Rijke, 1859). Lord Rayleigh proposed that when heat is added to the acoustic field when they are in phase, energy is added to the acoustic field in the chamber. However, the combustion becomes unstable when the added energy is greater than the damping/losses in the system as shown in equation 1.1. This criterion is used

to explain the cause of thermoacoustic instability.

$$R = \int_0^T \int_0^V p'(t)\dot{q}'(t)dtdV > \text{acoustic damping} \tag{1.1}$$

where R is the Rayleigh index, p' denotes acoustic pressure fluctuations at the flame, $\dot{q}'$ denotes the heat release rate fluctuations in the flame, t is the time variable, V denotes the control volume and T is the time period of the oscillations. In the equation 1.1, the left hand side represents the acoustic driving and right hand side refers to the acoustic damping.

Detrimental effects of thermoacoustic instabilty is seen in several gas turbine combustors, solid rocket motors, ramjets, scramjets etc. The notable incidents are the ones in F-1 engines that powered the Saturn rockets, solid-propellant rocket boosters used in the Minuteman intercontinental ballistic missile, and the Mars Pathfinder descent motor. Thermoacoustic instability cost billions of dollars to the aviation industry. Generally baffle plates are used to prevent the transverse mode of combustion instability. The tangential mode of combustion instability is seen in afterburners and is referred to as "screech" (Zinn and Lieuwen, 2005). Transverse mode of thermoacoustic instability is prevalent in gas turbine engines with high enough aspect ratios or there is large enough combustion source, operating in fuel-lean regimes to increase the fuel efficiency and the reduction of NOx emissions (Correa, 1993). All these modes of thermoacoustic instabilities cause structural damage to the engine and the vibrations can lead to the damage of the electrical components on board.

In the next section, we discuss a few important mechanisms that can cause thermoacoustic instability.

1.1.2 Mechanisms Responsible for Thermoacoustic Instability

As stated in Eq. 1.1, whenever the acoustic driving becomes greater than or equal to acoustic damping, thermoacoustic instability occurs. The saturation of the pressure oscillations occur when the acoustic driving is balanced by acoustic damping. There will be a growth (decay) in amplitude of p' when the acoustic driving (damping) dominates acoustic damping (driving). The sources for acoustic damping include viscous dissipation, radiative or convective heat transfer out of the combustor, transfer of acoustic en-

ergy within the acoustic modes etc., to name a few (Zinn and Lieuwen, 2005). However, the physical mechanisms responsible for the acoustic driving have to be understood to mitigate thermoacoustic instability.

Fluctuations in Flame Surface Area and Equivalence Ratio

In turbulent combustors, the turbulence in the underlying flow field affects the flame front (Renard *et al.*, 2000). Turbulence causes distortion and wrinkes in the flame surface which in turn affects the heat release rate fluctuations. The fluctuations in the flame surface area determines the heat release rate fluctuations. This modified heat release rate can enhance the acoustic fluctuations in the combustor, thereby causing thermoacoustic instability. Lieuwen *et al.* 1998 reported that the fluctuations in the equivalence ratio can cause thermoacoustic instability. The equivalence ratio fluctuations can cause improper mixing between fuel and air. The modulated reaction mixture which convects into the combustion chamber can cause periodic oscillations in the heat release rate, when in phase with the acoustic fluctuations, can act as acoustic driving mechanism.

Large Scale Coherent Vortices in the Flow Field

In addition to these, the flame stabilization mechanisms used to stabilize the flame in fuel lean conditions can result in large scale, coherent vortex shedding. These vortices contain the reaction mixtures and the sudden breakdown of these vortices can result in sudden heat addition in the combustion chamber, which can act as an acoustic driving mechanism (Schadow and Gutmark, 1992). Further, various studies reported the emergence of large scale coherent structures during the onset of combustion instability (Sampath and Chakravarthy, 2016; Unni and Sujith, 2017). Moreover, Chakravarthy *et al.* (Chakravarthy *et al.*, 2007) showed that the acoutic mode shifts to the hydrodynamic mode during thermoacoustic instability.

Other mechanisms

In spray combustors, the interaction of acoustic field with the atomization process causes fluctuations in the droplet size, evaporation times, mixing process which inturn affects the heat release rate. Thus, the spray-acoustic interaction can also result

in thermoacoustic instability (Crocco and Cheng, 1956; Sujith *et al.*, 2000). Complementing the above mentioned mechanisms, there are other mechanisms that can lead to thermoacoustic instability in a combustor. The similarity between time scales of various processes occuring in the combustor such as, the evaporation time scale, miximg time scale, convection time scale, acoustic time scale can lead to thermoacoustic instability if they satisfy eq. 1.1. The geometry of the combustor can modify the flow field which when interacts with the flame causes heat release rate fluctuations causing thermoacoustic instability (Zinn and Lieuwen, 2005). Unsteady combustion produces entropy waves in addition to acoustic waves. The entropy waves when accelerate past the combustor exit can generate acoustic waves (referred as indirect combustion noise). These waves can travel upstream and effect the flame, inturn effecting thermoacoustic instability (Lieuwen, 2003; Goh and Morgans, 2013).

Overall thermoacoustic instability occurs due to the interaction between the acoustic field, the hydrodynamic flow field and the reaction kinetics. This interaction is complex and highly nonlinear due to the inherent nonlinearity in turbulence, non-homogeneity of distribution of reaction species. Thus the onset of thermoacoustic instability is a nonlinear process and this can be seen in the saturation of acoustic oscillations.

1.1.3 Linear Stability Analysis

Thermoacoustic instability comprises of self-excited large amplitude limit cycle oscillations. In classical analysis, the onset of thermoacoustic instability is seen as the loss of dynamical stability in a combustor (Nair and Lieuwen, 2005; Thiruchengode, 2006). In order to perform linear analysis, the nonlinear partial differential equations are converted into ordinary differential equations. These equations are then linearized assuming that the fluctuations are small. The acoustic pressure fluctuations in gas turbine combustors are within 5% of the mean pressure (Lieuwen and Neumeier, 2002). Thus, the linear stability analysis is performed on the state space equations $\frac{dx}{dt} = Ax$, where A is the linear state space matrix and x is an array of system variables. The stability of the system is determined by computing the eigenvalues of A. During the dynamically stable regime, the real parts of all the eigen values will be negative. The linearly stable and unstable regimes are hence identified by the sign of the real parts of the eigen values.

Further, the linear stability of the combustor can also be determined using flame tranfer funtion (FTF). The forced response of the flame to the acoustic perturbarions at a forcing frequency is given by FTF. FTF measures linear reponse of the heat release rate fluctuations ($\dot{q}'$) to the acoustic velocity perturbations (u') at different forcing frequencies. The eigen values of FTF can then be used to idenfy the linear stability of the system.

In a linearly unstable system, when the steady state is perturbed, the amplitude of perturbations are expected to grow exponentially. However, in practical gas turbine combustors, during thermoacoustic instability, the acoustic oscillations saturate to limit cycle oscillations of finite amplitude. The classical linear stability analysis fails to determine the amplitude and frequency of these oscillations. We only get information about the growth and decay rate of these oscillations.

Further, linear stability analysis can only be applied when the fluctuations are small. The transition to thermoacoustic instability from combustion noise can be described using sub-critical and supercritical Hopf bifurcations. Nair *et al.* 2014 suggested that, in turbulent combustors, the transition to thermoacoustic instability occurs via subcritical Hopf bifurcation. Subcritical Hopf bifurcation contains a bistable zone where during a range of control parameter, when the perturbation is above a certain threshold, the system can transition to limit cycle oscillations even during a linearly stable regime. This phenomenon is called triggering. The classical stability analysis cannot explain triggering and triggering requires the presence of nonlinearities.

The nonlinear analysis to analyze the transition to thermoacoustic instability is explained in the section 1.3.

1.2 Historic Overview of Blowout

1.2.1 Literature Survey

When the flow velocity exceed the flame speed in a combustor, flame stabilization becomes a challenge. During flame blowout, the flame is convected downstream by the flow and ceases to exist in a combustor. Flame blowout has detrimental consequences in gas turbine engines. The notable incident of flame blowout is observed in SR-71 engine

during a high-acceleration turn where the flames are separated from the engine. Hence, determining the conditions of flame blowout is important to identify the operational regimes in a combustor.

Various studies reported conditions for the onset of flame blowout. Since flame blowout is studied as failure of flame stabilization, Zukoski and Marble 1955 developed a condition based on the flame holding mechanism. They proposed the Damkohlar number $Da = \tau_{res}/\tau_{chem}$, where τ_{res} denotes the time interval over which the incoming flow is in contact with the hot recirculation zone created by the flame holding devices and τ_{chem} denotes the ignition time. Thus $Da = 1$ is the condition for flame blowout. Similar studies are conducted by Longwell *et al.* 1953 and Splading 1955.

In literature, it is determined that the addition of H_2 causes a delay in the onset of blowout. The addition of H_2 increases $OH*$ radicals which increase the flame speed and reaction rate. Moreover, addition of H_2 also reduced the emissions of CO and NOx (Schefer, 2001; Griebel *et al.*, 2007).

The dynamics of the flame close to lean blowout limit is studied by Nair and Lieuwen 2005, Muruganandam *et al.* 2005. Nair and Lieuwen 2005 reported the occurrence of intermittent events localized in time close to flame blowout using the acoustic data and flame images. Muruganandam *et al.* 2005 developed precursors to flame blowout by measuring the OH^* chemiluminescence imaging. They demonstrated active control strategies on a swirl stabilized combustor.

The dynamics close to blowout and the physical process that causes blowout is explained in various studies (Nair and Lieuwen, 2007; Shanbhogue *et al.*, 2009; Muruganandam and Seitzman, 2012). They observed that as the equivalence ratio is reduced, we approach closer to the lean blowout limit, there is an increase in vorticity magnitude of the vortices near the bluff-body. The increase in vorticity increases flame stretch rates at some places. If the stretch rate exceed the flame extinction stretch rate, some holes are developed in the flame. A further reduction in equivalence ratio causes increase in the formation of holes. There will be violent detachment and attachment of the flame causing flame blowout. They observed that the vortices shed before blowout are due to von Karman type hydrodynamic instability. This flow-flame interaction will be non-linear and a nonlinear analysis of blowout could bring more insight into the dynamic processes prior to blowout of flame.

1.2.2 Classical Stability Analysis

The flame blowout is treated as the loss of static stability of the flame in contrast with the onset of thermoacoustic instability. Flame blowout is often treated as a flame stabilization problem. The occurrence of blowout is presaged by determining the conditions of lean blowout limit. Some of the conditions that determine the occurrence of flame blowout are given in previous section (Nair and Lieuwen, 2005; Muruganandam *et al.*, 2005).

However, all these conditions based on the flame stabilization mechanisms view blowout as an abrupt or instanteneous transition. In reality, blowout occurs due to the detachment and reattachement of flame due to flame stretch rates. The simple conditions mentioned above fail to explain the dynamics prior to blowout. Thus the classical linear stability analysis fails to give a complete picture of the onset of blowout.

Thus, we established the need for nonlinear analysis to analyze the transition to thermoacoustic instability and lean blowout. In the next few sections, we discuss two novel approaches to analyze these transitions : dynamical systems approach and complex systems approach.

1.3 Dynamical systems approach

Any system that evolves with time is a dynamical system. Dynamical systems theory is a branch to analyze the characteristics of the dynamical system. In the past few decades, dynamical systems theory is extensively applied to study various dynamical regimes exhibited by a thermoacoustic sytem by mainly analyzing the acoustic oscillations from the combustor.

Using dynamical systems theory, Jahnke and Culick 1994 proposed that a thermoacoustic system can undergo a pitchfork and torus bifurcation and exhibit quasiperiodic oscillations in addition to limit cycle oscillations. The quasiperiodic oscillation is characterized by the presence of two incommensurate dominant frequencies and their multiples and thus is not periodic. It has been shown that the acoustic oscillations can be treated using linear analysis but it is the heat release rate fluctuations that bring in the nonlinearitites. Fichera *et al.* 2001 demonstrated the presence of chaotic dynamics in

the heat release rate fluctuaions in lean gas turbine combustors.

1.3.1 Transitions to thermoacoustic instability and lean blowout

Various studies have used the approach of dynamical systems theory to characterize the nonlinear behavior of thermoacoustic systems and also to detect the dynamical transitions observed prior to the onset of thermoacoustic instability. With the help of dynamical systems approach, a rich dynamical behavior has been reported during the transition to thermoacoustic instability in such systems (Culick, 1994; Gotoda *et al.*, 2011; Juniper and Sujith, 2018; Kabiraj *et al.*, 2012; Gotoda *et al.*, 2014; Nair *et al.*, 2014). Kabiraj *et al.* 2012 showed the existence of various dynamical states such as quasiperiodic, chaotic, and period-k, in addition to limit cycle oscillations (LCO), in a premixed laminar thermoacoustic system.

In most of the turbulent combustors, as the equivalence ratio is varied from stoichiometric to fuel lean regimes, a transition in the system dynamics from low amplitude aperiodic oscillations (combustion noise) to large amplitude LCO (thermoacoustic instability) is observed. Lieuwen 2002 described the transition to thermoacoustic instability from combustion as the transition from fixed point to limit cycle oscillations. Traditionally, combustion noise was considered as mere stochastic fluctuations in the system. Nair *et al.* 2013 and Tony *et al.* 2015 used a plethora of tools to ascertain the deterministic nature of the signal and discovered that combustion noise has features of high dimensional chaotic oscillations contaminated with coloured and white noise. Nair *et al*. 2013 suggested that the transition from combustion noise to thermoacoustic instability can be considered as a transition from a chaotic state to an ordered state.

Nair *et al.* 2014 discovered that the transition to thermoacoustic instabilty occurs via intermittency, a state comprising of large amplitude limit cycle oscillations at irregular intervals amidst low amplitude aperiodic oscillations. Nair *et al.* 2013 mentioned the existence of type-II or type-III intermittency in the gaseous flame bluff body stabilized turbulent combustor. Nair and Sujith 2015 developed a model that captures the occurrence of intermittency prior to the onset of thermoacoustic instability, for a bluff body stabilized combustor using a stochasic kicked oscillator model. Seshadri *et al.* 2016 developed a model using the interaction between the acoustic field, vortex shedding

and the heat release rate. Detection of intermittency helped in developing precursors to thermoacoustic instability (Nair and Sujith, 2014).

After the occurrence of thermoacoustic instability, if the equivalence ratio is further reduced, we approach lean blowout limit. This transition from thermoacoustic instability to lean blowout exhibits rich dynamical behavior. Kabiraj *et al.* 2012 detected intermittency prior to blowout in laminar premixed combustion. In case of turbulent combustors, Unni and Sujith 2017 characterized the intermittency before and after the occurrence of thermoacoustic instability as type-II. Many other studies reported the occurrence of intermittent periodic bursts during the transition to thermoacoustic instability and to blowout (Unni and Sujith, 2015; Nair and Sujith, 2015; Thampi and Sujith, 2015; Nair *et al.*, 2014).

1.3.2 Synchronization transition to thermoacoustic instability

All the above analysis focuses on analyzing the acoustic signal alone. However, it is well known that the coupled interaction between p' and $\dot{q}'$ causes thermoacoustic instability (Rayleigh, 1878). Various studies in the past have focused on this coupled interaction during either the stable or the unstable regimes of combustor operation (Rogers and Marble, 1956; Keller *et al.*, 1982; Smith and Zukoski, 1985; Poinsot *et al.*, 1987; Macquisten and Dowling, 1993; Yu and Monkewitz, 1990; Broda *et al.*, 1998; Venkataraman *et al.*, 1999; Guethe *et al.*, 2012; Sivakumar and Chakravarthy, 2008). Recently, such coupled interaction between p' and $\dot{q}'$ at various dynamical states during the transition from combustion noise to thermoacoustic instability via intermittency was analyzed by Pawar *et al.* 2017 and Mondal *et al.* 2017.

Pawar *et al.* 2017 applied synchronization framework to characterize the temporal behavior of the coupled p' and $\dot{q}'$ in a turbulent combustor. They cast the chamber acoustic field (p') and the turbulent reactive flow ($\dot{q}'$) as oscillators to apply synchronization framework to thermoacoustic system, as these oscillators exhibit self-sustained oscillations under the influence of turbulent flow (see Appendix for more details). Using tools from synchronization theory, they described that the transition to thermoacoustic instability happens from a state of desynchronized aperiodicity (combustion noise) to the states of phase synchronized (PS) and generalized synchronized (GS) periodic os-

cillations. Phase synchronization refers to a state when the oscillators are phase locked and the state of Generalized synchronization refers when the oscillators are related by functional relationship. Such a transition to PS is observed to occur via a state of intermittent phase synchronization (IPS). However, in their study, the characterization of these states was mostly qualitative. Characterization of spatiotemporal behavior of the coupled acoustic field and local heat release srate fluctuations in the reaction field during the intermittency route to thermoacoustic instability was performed by Mondal *et al.* 2017. They observed that the transition from combustion noise (phase asynchornous state) to thermoacoustic instability (phase synchronous state) occurs through the formation of a chimera-like state where the phase asynchronous and the phase synchronous regions coexist at the same instant in the reaction field. They observed that the Kuramoto order parameter indicates the synchronization transition at the onset of thermoacoustic instability. Chiocchini *et al.* 2017 characterized the nature of coupling between p' and $\dot{q}'$ during the onset of thermoacoustic instability. They reported that a chaotic synchronization index, namely interdependence index can detect the onset of thermoacoustic instability. They also found that the dependence of p' on $\dot{q}'$ is higher than vice versa and that the heat release rate acts as a driving subsystem. They suggested that, while the asymmetry in the interdependence index implied the presence of an unidirectional coupling between p' and $\dot{q}'$, in reality this cannot be true. They attributed this anomaly to the difference in the intrinsic embedding dimensions of the pressure and the heat release rate oscillations which cannot be accommodated in the computation of the interdependence index. We hypothesize that this anomaly observed due to interdependence index is not merely because of the difference in the intrinsic embedding dimensions, but might also be due to the asymmetric bidirectional coupling between acoustic pressure and unsteady heat release rate. Hence, there exists a need for a detailed quantitative analysis to detect the synchronization transition and for the characterization of the directional dependence between p' and $\dot{q}'$.

1.4 Complex systems approach

The nonlinear interactions between the acoustic field, the hydrodynamic field and the unsteady combustion resulting in different dynamical regimes varying from combustion noise (chaos) to thermoacoustic instability (order) in a combustor suggest that the

thermoacoustic system can be treated as a complex system. In a complex system, the interaction between components is nonlinear such that the collective behavior of the system is more than sum of their individual behaviors. These components can self-organize and exhibit a coherent behavior (Johnson, 2002). This phenomenon is called emergence in complex system (Mitchell, 2006). We presume that the emergence of thermoacoustic instability (order) from combustion noise (chaos) and the appearance of discrete scales during thermoacoustic instability in contrast to the multiple scales present during combustion noise might be due to self-organization in the system. The traditional reductionist approach which monitors the individual element is no longer sufficient to describe the emergent behavior of complex systems (Barabási, 2011).

In complex systems approach, Nair and Sujith 2013 performed multifractal analysis on the acoustic time series acquired from a tubulent combustor. They detected multifractal nature of combustion noise and the collapse of multifractal spectrum during the onset of thermoacoustic instability. The presence of multifractal spectrum shows the lack of a single characteristic temporal scale during combustion noise. Self-similar nature is reported in the oscillations prior to blowout (Gotoda *et al.*, 2012; Domen *et al.*, 2015) using measures such as permutation entropy, fractal dimension and short-term predictability. Further, Unni and Sujith 2015 developed a unified framework to describe the transition from combustion noise to thermoacoustic instability and to lean blowout. Using complex systems approach, an important precursor, Hurst exponent is developed.

1.4.1 Complex networks to analyze complex systems

Complex networks are used to study complex systems as they help in understanding the connectivity pattern (Lesne and Laguës, 2011). Complex networks comprise of nodes which represent the components of the system and links representing the interactions between these components. The topology and the measures derived from a network can be used to characterize the qualitative and quantitative behavior of a complex system. Variation in the dynamics of the system is reflected in the topology of the network. The measures derived from the networks can be used to analyze the transitions in the dynamics of these systems. The underlying dynamics of a physical system is preserved in the time series data. Hence, in order to study complex systems, time series from such

systems is converted into complex networks. Modeling the network structure is crucial to understand the underlying dynamics of the system. Many methods have been devised to convert the time series into complex networks (Xu *et al.*, 2008; Lacasa *et al.*, 2008; Zhang and Small, 2006; Donner *et al.*, 2011). Strozzi *et al.* 2009 have shown that time series can be converted into complex networks and vice versa.

Recently, complex networks are implemented to analyze fluid flows (Gao and Jin, 2009; Gao *et al.*, 2010; Charakopoulos *et al.*, 2014). The network topologies of the complex networks constructed from thermoacoustic system can enable us to provide an alternate description for the transition from combustion noise to thermoacoustic instability and to lean blowout. Okuno *et al.* 2015 used the cyclic networks and found that the thermoacoustic oscillations possess pseudo-periodicity, high-dimensional nature, power-law behavior in the degree distribution and small-world like nature. In addition to these, Murugesan and Sujith (Murugesan and Sujith, 2015) introduced complex networks to analyze the dynamical regimes in thermoacoustic system. They used visibility algorithm to convert the time series to complex networks. They detected scale-free behavior during combustion noise and regularity at the onset of thermoacoustic instability. Further, Murugesan and Sujith (Murugesan and Sujith, 2016) showed that the quantities derived from complex networks such as characteristic path length, clustering coefficient, network diameter and global efficiency can be used as precursors to predict thermoacoustic instability and blowout.

While converting time series into complex network using visibility algorithm, information related to the geometry and structure of the attractor is lost. In order to preserve the geometric characteristics of the attractor, we use $\varepsilon-$recurrence networks (RN). RN preserves the information related to the geometry of the attractor.

In the present work, we analyze the dynamical transitions in a turbulent combustor using recurrence networks. We attempt to develop precursors and characterize the dynamical regimes using the properties of the network topology.

1.5 Precursors to Thermoacoustic Instability and Lean Blowout

Thermoacoustic instabilty and lean blowout are hazardous to the combustors. Hence, it is important to forewarn the occurrence of these impending instabilities and also to prevent them. In order to mitigate the transition to thermoacoustic instability and lean blowout, several passive and active control strategies are developed. In this section we focus on various measures that can be used as early warning signals to predict these instabilities.

In the recent past, several linear and nonlinear measures are developed. Nair and Sujith 2013 and Unni and Sujith 2015 demonstrated that the Hurst exponent can be used as an early warning measure for thermoacoustic instability and blowout. In their subsequent work, they used recurrence quantification analysis on time series of acoustic pressure and found that recurrence measures can be used as precursors (Nair *et al.*, 2014). We discuss about recurrence and recurrence analysis in the chapter 2.4. Unni *et al.* 2015 applied an anomaly measure from symbolic time series analysis to detect the onset of thermoacoustic instability.

Nair and Lieuwen 2005 developed precursors for the blowout detection based on spectral, statistical and threshold-based analysis of the acoustic signal. Muruganandam *et al.* 2005 used OH^* chemiluminescence to obtain blowout precursors. Using dynamical system and complex system approach, Gotoda *et al.* 2012 demonstrated that various nonlinear quantities such as translational error and permutation entropy can be used as early warning signals to predict blowout. Unni and Sujith 2015 demonstrated that Hurst exponent can also be used as a precursor to blowout.

Using the measures obtained from visibility network, Murugesan and Sujith 2015; 2016 developed precursors to thermoacoustic instability and blowout.

1.6 Objectives and Overview of the Thesis

The objectives of the present thesis are focused on the analysis of the transition from combustion noise to thermoacoustic instability and lean blowout using recurrence networks and also focused on understanding the coupled behavior of acoustic field and the

unsteady flame dynamics during the onset of thermoacoustic instability. The outstanding questions are identified and the objectives of the present thesis are summarized as follows.

1. We investigate the transition from combustion noise to thermoacoustic instability and lean blowout using recurrence networks. Recurrence networks preserve the geometry of the attractor. We idenfity the degree distribution of the network during the transition to thermoacoustic instability and lean blowout. We show the presence of power laws in the degree distributions of recurrence networks constructed from combustion noise and oscillations prior to lean blowout. Power laws in the degree distributions represent the presence of singularities in phase space.

2. We investigate the transition of system dynamics from combustion noise to thermoacoustic instability and blowout. We derive the network properties and show that they can be used as precursors to detect the onset of thermoacoustic instability and lean blowout.

3. Pawar *et al.* 2017 introduced synchronization framework to analyze the transition to thermoacoustic instability. We construct multivariate recurrence networks namely, joint recurrence and cross recurrence networks. We show that the multivariate recurrence plots capture the coupled behavior of the acoustic field and the unsteady heat release rate during the transition to thermoacoustic instability. We further quantify the synchronization transition and identify the onset of various states through the measures derived from the recurrences in phase space.

4. In order to investigate the interaction between the acoustic field and the unsteady flame dynamics, we identify the coupled behavior between p' and $\dot{q}'$ using measures derived from intersystem recurrence networks. We discover an asymmetrical bidirectional coupling where $\dot{q}'$ affects p' than vice versa. This finding paves way to design effective control strategies to mitigate thermoacoustic instability.

The organization of the thesis is presented as follows.

In **Chapter 2**, a basic introduction of complex networks and the methods to construct complex networks from time series is given. Mainly, the description of recurrence networks and the measures derived from recurrence networks is given. The extension of univariate recurrence networks to multivariate recurrence networks and the corresponding implications of the measures in analyzing the coupled behavior is also provided. A brief overview of recurrence quantification analysis and a few synchronization tools based on recurrences in phase space is also summarized.

Chapter 3 summarizes the descriptions of experimental setups used in the present study. Primarily the data acquisition process of the acoustic fluctuations and the global heat release fluctuaions from a bluff body stabilized turbulent combustor is summarized. The experimental setup is same as the one used by (Pawar *et al.*, 2017; Unni and Sujith, 2015).

The recurrence network analysis of thermoacoustic system is given in **Chapter 4**. The unsteady pressure data which are same as the one reported by Unni and Sujith 2015 are used in the network analysis. The network topolgies for all the dynamical regimes are shown. The degree distributions and other network measures such as characteristic path length and betweenness centrality are found to detect the transtions.

The coupled behavior of acoustic pressure and heat release rate oscillations for the transition of a thermoacoustic system from combustion noise to thermoacoustic instability through intermittency is quantified using multivariate recurrence plots and recurrence networks in **Chapter 5**. The synchronization states are detected using the measures derived from these networks. The directional dependence between the acoustic pressure and heat release rate oscillations is determined.

Finally, conclusions derived from the present thesis are provided in **Chapter 6**. This chapter also includes the scope for future work based on the use of recurrence networks to thermoacoustic systems.

CHAPTER 2

BACKGROUND ON COMPLEX NETWORKS

In this chapter, we provide a brief description of complex networks, various network construction techniques and the measures derived from network topology. An insight into the characteristics of scale free networks, small world networks and the presence of power laws in the degree distributions of the network is provided. Further, we describe the procedure for construction of complex networks from time series.

This chapter mainly focuses on the construction of recurrence networks and interpreting the network mesures used to quantify the recurrence networks such as degree distribution, characteristic path length, betweenness centrality etc. An extension of univariate recurrence networks to bivariate recurrence networks such as joint recurrence networks and cross recurrence networks which will help in investigating synchronization phenomenon between two oscillators. We also mention a few synchronization measures which are based on recurrences in phase space.

2.1 Historic overview

We see networks everywhere. Social networks, ecological networks, transportation networks, brain networks, climate networks etc., are a few examples. Network are constructed based on interactions between several components in a system. If these interactions give rise to emergence of self organization, we can consider the system as complex system and the networks constructed are called complex networks (Bar-Yam, 1997). To summarize the importance of complex networks in the words of an expert in the field of complex networks, Barabasi 2011 "Therefore, if we are ever to have a theory of complexity, it will sit on the shoulders of network theory."

Network science is based on graph theory and statistical physics. Networks consist of nodes with edges between them. Euler in 1736, made the first use of graph theory to solve the infamous KÃűnigsberg bridge problem. The use of complex networks became

extensive after the discovery of scale free (Barabási and Albert, 1999) and small world networks (Watts and Strogatz, 1998). The discovery of small world networks came as an answer to the question "How small is the world?" Milgram 1967 showed an average of six degrees of separation between any two people in the world.

Watts and Strogatz 1998 developed a model for constructing small world network and identified the difference between a random network (where two nodes are connected randomly using a probability) and a regular network (all the nodes are connected to each other). Small world networks are observed in brain networks, power grids, metabolic reaction networks, protein-protein interaction networks and scientific co-authorship networks (Boccaletti *et al.*, 2006).

Barabasi and Bonabeau 2003 discovered scale free networks and reported that world wide web, airport networks, internet, research collaborations have a very inhomogeneous connectivity pattern setting them apart from regular and random networks. They observed that a few nodes have very high connections (hubs) whereas a large number of nodes have few connections but are connected to the hubs. The degree distribution of scale free networks follow a power law $P(k) = k^{-\gamma}$, where $P(k)$ is the probability of finding a node with k connections. The scale free networks are very robust to random attack but quite susceptible to targeted attack on hubs.

Hence, the network topology can reveal complex characteritics of the system which are different from a regular and a random network. We now discuss the various methods to construct networks from time series.

2.2 From Time Series To Complex Networks

Time series is a reflection of the complex spatiotemporal behavior observed in the system. The topologies of the networks constructed from the timeseries acquired from a complex system help unveil information about the collective behavior and identify any hidden patterns in networks.

There are several methods to construct time series into complex networks. The construct techiniques involve cyclic networks, k-nearest neighbourhood methods, visibility networks, recurrence networks etc., to name a few. Zhang and Small 2006 constructed

cyclic networks from pseudo-periodic time series. The networks are constructed based on temporal correlations between two cycles in the time series. Lacasa *et al.* 2008 and Luque *et al.* 2009 introduced visibility and horizontal visibility graphs. The networks are constructed from the peaks of time series, if they satisy a visibility criterion. The network measures are related to the fractal dimension of the timeseries.

Donner $etal.$ 2011 introduced recurrence networks. The networks are constructed based on a propery, recurrence, a fundamental property of any deterministic dynamical system. The network is constructed based on the recurrence of state space vectors reconstructed from a time series. While converting time series into complex network using visibility algorithm, information related to the geometry and structure of the attractor is lost. In order to preserve the geometric characteristics of the attractor, we use $\varepsilon-$recurrence networks (RN). Further, as recurrence is a fundamental property of any dynamical system, the rationale behind constructing complex networks from time series using recurrence networks is natural and simple than visibility networks (Marwan *et al.*, 2009). RN does not depend on temporal correlations explicitly. Thus RN is more robust than other methods that consider temporal correlations, in cases where there is external noise in the system. Constructing RN from a time series requires lesser number of data points than those required for computing Lyapunov exponent. Hence, measures derived from RN are well suited to discriminate between chaotic and periodic state compared to Lyapnov exponent when a shorter time series is available (Donges *et al.*, 2011).

By considering the advantages of RN, we use RN in present study. The subsequent sections provide a brief description of network construction technique.

2.3 Recurrence Networks

There are several methods to generate complex networks from a time series. ε- recurrence method is one of them. In this method, we compute the recurrences of phase space vectors after reconstructing the phase space using Takens embedding theorem (Takens, 1981). The discretely sampled experimental time series $x(1), x(2), ...x(N_T)$ is embedded in an *M*-dimensional phase space using an appropriate time delay, where N_T

is the total number of points in the time series. The delay vectors are given by

$$X(t_i) = x(i), x(i+\tau), ..., x(i+(M-1)\tau) \tag{2.1}$$

In this paper, the embedding dimension *M* is chosen using Cao's algorithm (Cao, 1997). The first minimum of the average mutual information is chosen to be the time delay for computing delay vectors from the discretely sampled time series.

A state (phase space vector) $X(t_i)$ is said to be recurrent if there are t_i and t_j such that $d(X(t_i), X(t_j)) < \varepsilon$ where $d(X(t_i), X(t_j))$ is the distance between the phase space vectors $X(t_i)$, $X(t_j)$ computed using the Euclidean norm. Under general conditions, the structure of recurrences in phase space can be encoded in the recurrence matrix (Eckmann *et al.*, 1995; Marwan *et al.*, 2007).

$$R_{i,j} = \theta\left(\varepsilon - \|X(t_i) - X(t_j)\|\right) \tag{2.2}$$

Here, θ is the Heaveside function.

There are some quantification measures derived from recurrence matrices to quantify the dynamics of the time series. The analysis is called as recurrence quantification analysis (RQA). We shall discuss a few measures in the section 2.3.

We consider only spatial interdependencies in recurrence networks. To construct the recurrence network from the time series, we use the adjacency matrix constructed using recurrence matrix according to the relation,

$$A_{i,j} = R_{i,j} - \delta_{i,j} \tag{2.3}$$

The adjacency matrix provides the information regarding the nodes and the connections between them. If $A_{i,j} = 1$ then the nodes *i, j* are connected, which implies that the state space vectors are in a proximity of recurrence threshold ε in the phase space.

The measures derived from recurrence matrix characterizes the dynamical properties of phase space trajectories in contrast to the measures derived from RN which describe the geometrical properties of the attractor. A dynamical property characterizes the dynamics of the system i.e,. regular or irregular dynamics whereas a geometrical

property characterizes the geometry and structure of the reconstructed phase space. The main advantage of recurrence network is that it provides additional measures from networks to characterize the geometric properties of the attractor and hence provides more tools for the analysis of time series (Marwan and Kurths, 2015).

A crucial parameter in constructing the network is the recurrence threshold ε. If the threshold is very large, the network becomes very dense as there are too many links leading to false recurrences. On the other hand if the recurrence threshold is too small, the network breaks down into mutually disjointed components. Hence the network characteristics can become ambiguous. The recurrence threshold is chosen by the approach proposed by Jacob *et al.* 2016 which determines an admissible range for ε. Hence, the choice of the recurrence threshold is not arbitrary.

In the next subsection, we provide a brief description of the measures derived from RN such as degree distribution, characteristic path length and betweenness centrality.

2.3.1 Measures describing the topological properties of the network

The following measures are computed from the adjacency matrix A which encodes the information related to the connectivity of each node (Donner *et al.*, 2011).

Degree Distribution

Degree distribution is the graph plotted between $P(k)$ and k where $P(k)$ is the probability of a given node to have a degree k. $P(k)$ is given by $n(k)/N$ where $n(k)$ is the number of nodes having the degree k and N is the total number of nodes. The degree of a node k_i represents the connectivity of the node. The degree of a node i is the sum of all the elements in the i^{th} row of Adjacency matrix. As the topology of RN represents the structure of the attractor, local connectivity is related to local phase space density of the attractor (Donner *et al.*, 2011). Thus, the variation in the degree distribution reflects the variation of the local phase space density over the attractor.

Betweenness centrality

Betweenness centrality computes the fraction of shortest paths passing through a vertex (node).

$$b_v = \sum_{i,j \neq v}^{N} \frac{\hat{\sigma}_{i,j}(v)}{\hat{\sigma}_{i,j}} \tag{2.4}$$

where, $\hat{\sigma}_{i,j}$ gives the number of shortest paths between two nodes i and j. $\hat{\sigma}_{i,j}(v)$ gives the number of shortest paths between the nodes i and j that are passing though the node v. Betweenness centrality determines bottleneck nodes or the regions of low phase space density that connect two regions of high phase space density.

Characteristic path length

Characteristic path length is the average of the length of the shortest paths between two nodes.

$$CPL = \frac{1}{N(N-1)} \sum_{i,j-1}^{N} d_{i,j} \tag{2.5}$$

where $d_{i,j}$ is the length of the shortest path between a pair of nodes (*i, j*) which is nothing but the minimum number of links between node i and node j. We do not consider disconnected nodes while calculating CPL.

2.4 Analysis of coupled behavior using bivariate recurrence plots and networks

The coupled behavior of two oscillators is studied using the multivariate recurrence matrices ((Romano *et al.*, 2004)). The univariate recurrence matrix R can be extended as joint and cross recurrence matrices to study the coupled behavior of the oscillators.

The joint recurrence matrix (JRM) is computed by the element-wise multiplication of the individual recurrence matrices (R^X, R^Y) of the two oscillators X and Y. If the delay vectors of the two oscillators are denoted by V and W, respectively, then

$$JRM_{ij} = \Theta(\epsilon_V - \|V_i - V_j\|)\Theta(\epsilon_W - \|W_i - W_j\|) \tag{2.6}$$

JRM captures the presence of simultaneous recurrences of the phase trajectories of both the oscillators. If the states V_i and W_i recur simultaneously, then JRM_{ij} = 1; otherwise JRM_{ij} = 0.

The cross recurrence matrix (CRM) compares the states of the two oscillators in the same reconstructed phase space, and is computed as follows

$$CRM_{ij} = \Theta(\epsilon_{VW} - \|V_i - W_j\|) \tag{2.7}$$

CRM captures the presence of similar states in both the oscillators. If CRM_{ij} = 1, then the state of one oscillator recurs to the state of the other oscillator. Unlike R and JRM, the CRM is not necessarily symmetric. The threshold (ϵ_{VW}) is chosen such that the cross recurrence rate is fixed.

In order to link the recurrent behavior of two oscillators to detect synchronization between them, a measure of probability of recurrence $P(\tau)$, also referred to as τ - recurrence rate, was introduced by Romano *et al.* 2005. $P(\tau)$ measures the probability with which a given state vector of the trajectory of a single oscillator recurs after a time lag τ.

$$P(\tau) = \frac{1}{N-\tau} \sum_{i=1}^{N-\tau} \Theta(\epsilon_V - \|V_i - V_j\|) \tag{2.8}$$

The type of synchronization is characterized based on the locking of the location of the peaks as well as their heights in the $P(\tau)$ plots of the two oscillators. Further details on the use of probability of recurrence plots to detect the synchronization states in thermoacoustic system are given in Pawar *et al.* 2017.

2.4.1 Measures to quantify the coupled behavior of oscillators using recurrence plots

Determinism (DET)

Determinism (DET) measures the percentage of recurrence points in a recurrence matrix which form diagonal lines of minimum length l_{min}.

$$DET = \frac{\sum_{l=l_{min}}^{N} lF(l)}{\sum_{l=1}^{N} lF(l)} \tag{2.9}$$

where $F(l)$ is the frequency distribution of the lengths of the diagonal lines and N is the number of state vectors in the reconstructed phase space. When the dynamics is periodic, RP comprises only of diagonal lines and hence DET attains the maximum value of 1. Thus, DET can be used to detect the occurrence of periodic and quasiperiodic dynamics in the system.

Recurrence rate (RR)

Recurrence rate (RR) measures the average number of recurrences present in a recurrence matrix, R

$$RR = \frac{1}{N^2} \sum_{i,j=1}^{N} R_{ij} \tag{2.10}$$

RR attains the maximum value of 1 when all the state vectors are recurring in the reconstructed phase space. We fix RR of the recurrence matrices of p' and $\dot{q}'$ to compare across different states.

Correlation of probability of recurrence (CPR)

Correlation of probability of recurrence (CPR) is the cross correlation of the probability of recurrences of the two oscillators.

$$CPR = \frac{\left\langle \bar{P}_1(\tau > \tau_c)\bar{P}_2(\tau > \tau_c) \right\rangle}{\sigma_1 \sigma_2} \tag{2.11}$$

Here, $\bar{P}_1$ and $\bar{P}_2$ are the mean subtracted values of P_1 and P_2, and σ_1, σ_2 are the standard deviations of $\bar{P}_1(\tau)$ and $\bar{P}_2(\tau)$, respectively. We use the modified form of CPR

proposed by Goswami *et al.* 2012 and consider only those lags (τ) which are greater than the lag (τ_c) at which the autocorrelation of the signal is lesser than $1/e$ to exclude the effect of autocorrelation. The value of CPR ranges between -1 and 1. If both the oscillators are phase synchronized, then the location of the peaks of both $P_1(\tau)$ and $P_2(\tau)$ coincide. Hence, the CPR reaches its maximum (closer to 1) and can be used as an index to detect PS (Romano *et al.*, 2005).

Joint probability of recurrence (JPR)

Joint probability of recurrence (JPR) is the average probability of joint recurrences in time, whose value can be obtained as follows

$$JPR = \frac{\frac{RR_J}{RR} - RR}{1 - RR} \tag{2.12}$$

where RR_J is the joint recurrence rate and RR is the recurrence rate of the individual recurrence matrices. The joint recurrence rate is given by,

$$RR_J = \frac{1}{N^2} \sum_{i,j=1}^{N} JRM_{ij} \tag{2.13}$$

During the regime of generalized synchronization (GS), we expect similar value of RR_J as that of individual RR of both the oscillators. Hence, JPR becomes closer to 1 during the GS state and can be used as an index to detect the GS state (Romano *et al.*, 2005).

All the above measures are based on the individual and joint recurrence matrices computed from the time series of coupled oscillators. We now describe measures derived from the joint and cross recurrence networks. These networks are based on geometric signatures of the attractors in the phase space.

2.4.2 Measures to quantify the coupled behavior using recurrence networks

We construct recurrence networks from recurrence matrices**?**. The adjacency matrix (A_{ij}) is computed from R_{ij} as follows

$$A_{ij} = R_{ij} - I_{ij} \tag{2.14}$$

where I_{ij} is the identity matrix, i.e. we subtract the identity matrix from the R to discount self connected nodes in the network. The nodes in the recurrence network correspond to the state vectors in the reconstructed phase space. Two states are connected with a link, if they recur.

For studying the coupled behavior of two oscillators, networks are constructed from JRM and CRM, respectively. The measures computed from the recurrence networks are described below.

Network transitivity $(\mathcal{T})$

Network transitivity computes the number of closed triangles in a network given that two among those three nodes are connected (Newman, 2003).

$$\mathcal{T} = \frac{\sum_{i,j,k=1}^{N} A_{ij}A_{jk}A_{ki}}{\sum_{i,j,k=1}^{N} A_{ij}A_{jk}} \tag{2.15}$$

In order to study the coupled behavior of two oscillators, the joint transitivity $(\mathcal{T}_J)$ is used, which is the transitivity of the joint recurrence network. During GS, $\mathcal{T}_J$ is high due to the increase in the occurrence of simultaneous recurrences. Feldhoff *et al.* (Feldhoff *et al.*, 2013) introduced a normalized measure, the transitivity ratio $(Q_{\mathcal{T}})$, which is the ratio of joint transitivity to the individual transitivities, $\mathcal{T}_X$ and $\mathcal{T}_Y$ of the two oscillators X and Y.

$$Q_{\mathcal{T}} = \frac{2\mathcal{T}_J}{\mathcal{T}_X + \mathcal{T}_Y} \tag{2.16}$$

Here, $Q_{\mathcal{T}}$ will reach its maximum (around 1) during the occurrence of GS and hence can be used as an index to detect GS.

Cross transitivity

Cross transitivity, $\mathcal{T}_{XY}$, is the probability that two nodes in the recurrence network of the second oscillator (Y) are connected given that they are neighbors to a node in the recurrence network of the first oscillator (X). In other words, it measures the number of triangles with two vertices in one network and the third vertex in the other network (Feldhoff *et al.*, 2012). The interlinks between the two networks are obtained using CRM. CRM is not necessarily symmetric and hence, $\mathcal{T}_{XY}$ need not be the same as $\mathcal{T}_{YX}$. This inequality can be used to characterize the directional dependence of the two oscillators (Feldhoff *et al.*, 2012).

CHAPTER 3

EXPERIMENTAL SETUPS AND MEASUREMENT TECHNIQUES

In this chapter, we provide a description of the experimental setup and various measurement techniques. e perform experiments on a laboratory-scale backward facing step turbulent combustor. We systematically vary the control parameter (air flow velocity andd equivalence ratio (ϕ)) and study the dynamics at different dynamical states of combustor operation. We acquire the acoustic data using a pressure transducer and spatially averaged global heat release rate using photomultipler tube (PMT). The experimental setup is same as the one used by (Pawar *et al.*, 2017; Unni and Sujith, 2015).

3.1 Experimental rig : TARA

Setup Description

The experiments were conducted in a laboratory scale combustor having a partially premixed turbulent flame as shown in Fig. 3.1. The setup is named as TARA Thermo-Acoustic Rig for Axial Instability).The experimental setup consists mainly of three parts: i) a settling chamber, ii) a burner, and iii) a combustor. The air is first passed through the settling chamber, which reduces the unsteady hydrodynamic fluctuations and eddies at the air inlet from the flow inside the combustion chamber. In the burner, fuel (Liquefied Petroleum Gas; propane 40% and butane 60% by volume) is partially mixed with the incoming airflow from the settling chamber at different equivalence ratios. This partially premixed fuel-air mixture then enters into the main combustor section. The combustor is a rectangular duct which is 1400 mm long and 90 mm $\times$ 90 mm wide, and has a backward facing step (dump plane) at the inlet. A bluff body, circular disc of diameter 47 mm and thickness 10 mm, is located at a distance of 4.5 mm from the inlet of the combustor.

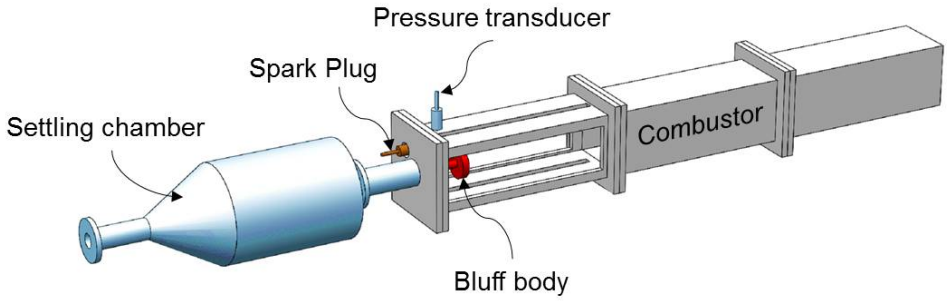

Figure 3.1: A schematic of the bluff body stabilized turbulent flame combustor.

The air and fuel flow rates are controlled separately by using mass flow controllers (Alicat Scientific, MCR 2000SLPM - for air, and MCR 100SLPM - for fuel; uncertainty is $\pm 0.8\%$ of measured reading $+0.2\%$ of full-scale reading) in the system. In bluff body combustor, the fuel flow rate is maintained at a constant value of 25 slpm and the air flow rate is varied from a value of 400 slpm to 940 slpm such that the flow field in the system is turbulent ($Re = 1.09 \times 10^5$ to $Re = 2.12 \times 10^5$) throughout the experiment. The estimated uncertainties in Re are $\pm 1.97 \times 10^3$ to $\pm 2.71 \times 10^3$. The equivalence ratios range from 0.95 ± 0.02 to 0.46 ± 0.01. In swirl combustor, the fuel flow rate is maintained at a constant value of 21 slpm and the air flow rate is varied from a value of 330 slpm to 950 slpm. For the purpose of initial ignition, a spark plug (along with 11 kV ignition transformer - National Engineering Corporation), fixed at the dump plane, is used to ignite the combustible air-fuel mixture. Quartz windows of size 90 mm $\times$ 360 mm, located on both the side walls of the combustor, provide optical access required for the measurement of heat release rate fluctuations from the flame.

Measurements and Data Acquisition

We measure the acoustic pressure fluctuations (p') from the combustor using a piezo-electric transducer (PCB Piezotronics, PCB103B02, with a sensitivity of 223.4 mV/kPa, and an uncertainty of ± 0.15 Pa). The pressure transducer is fixed on the top wall near the inlet step of the combustor. This position of the transducer corresponds to a near maximum amplitude of the acoustic pressure in the duct. It is an appropriate location for the measurement of the acoustic pressure in this combustor, as it always remains a pressure antinode for all the acoustic modes of the duct. The unsteady heat release rate fluctuations ($\dot{q}'$) are captured by using a photomultiplier tube, PMT, (Hamamatsu

H10722-01). A CH* bandpass filter (wavelength = 432 nm and 10 nm FWHM), which captures the CH^* chemiluminescence intensity from the flame, is used to filter the input to the PMT. The chemiluminescence intensity thus recorded is a measure of the heat release rate from the flame. The PMT is positioned at a distance 500 mm normal to the combustor wall near the location of the bluff body. The signals of the pressure fluctuations and the heat release oscillations were acquired for 3 s at a sampling frequency of 10 kHz. A 16-bit analog to digital (NI-6143) card is used for the data acquisition. Since our main objective in the present study is to analyze the synchronization characteristics of p' and $\dot{q}'$, we directly use the raw (mean subtracted) signals obtained in voltage from the pressure transducer and the PMT throughout our analysis.

CHAPTER 4

ANALYSIS OF TRANSITIONS TO THERMOACOUSTIC INSTABILITY AND BLOWOUT USING RECURRENCE NETWORKS

The present chapter discusses the complex network approach to unravel the pattern or dynamical features in the dynamics of the thermoacoustic systems. The transition to thermoacoustic instability and blowout are investigated. First, the scale invariance of combustion noise generated from turbulent reacting flows in a confined environment is investigated using complex networks. The time series data of unsteady pressure, which is the indicative of spatio-temporal changes happening in the combustor, is converted into complex networks using the visibility algorithm which is explained in the previous chapter. We examine the presence of powerlaw behaviors in the degree distributions of the RNs constructed during various dynamical regimes. The topological measures such as characteristic path length and betweenness centrality are evaluated to quantify the changes in combustion dynamics. These topological measures of networks that vary significantly well before the transition to flame blowout are used as the precursors to detect an impending blowout in the combustion systems.

4.1 Time Domain Analysis of Acoustic Pressure Fluctuations

We observe the transitions from combustion noise to thermoacoustic instability and then to lean blowout as the equivalence ratio (ϕ) is varied. We varied the equivalence ratio (ϕ) from 0.98 to 0.29 in this study. When the equivalence ratio is closer to 1, we observe combustion noise and when we approach the equivalence ratio of 0.29,

The results presented in this chapter are published in V. Godavarthi, V. R. Unni, E. A. Gopalakrishnan, R. I. Sujith, Recurrence networks to study dynamical transitions in a turbulent combustor *Chaos: An Interdisciplinary Journal of Nonlinear Science*, 27(6), 063113. (2017).

blowout occurs. The time series of acoustic pressure is plotted for various equivalence ratios in Fig. reffig.2. When the equivalence ratio is 0.98, we observe combustion noise composed of aperiodic fluctuations (Fig. 5.2(a)). When the equivalence ratio is 0.8, we observe intermittency (Fig. 5.2(b)) which consists of large amplitude periodic fluctuations amidst aperiodic oscillations. The equivalence ratio is reduced to 0.77 (Fig. 3c), the number of intermittent bursts is increased and the onset of periodic oscillations can be seen when the equivalence ratio is further reduced to 0.74 (Fig. 5.2(d)). As the equivalence ratio is further reduced to 0.5, we observe thermoacoustic instability (Fig. 5.2(e)). On further reduction of equivalence ratio to 0.47, we observe that intermittency sets in (Fig. 5.2(f)). The equivalence ratio is further reduced to 0.44, the amplitude and the duration of the periodic bursts in intermittency is decreased (Fig. 5.2(g)). When the equivalence ratio is reduced to 0.29, we observe low amplitude aperiodic oscillations (Fig. 5.3(h)). If we reduce the equivalence ratio further, the flame blows off.

Thus, as we progress from combustion noise to thermoacoustic instability, the periodicity of the signal increases. We also observe that on further reduction of equivalence ratio, during the transition from thermoacoustic instability to lean blowout, the periodicity of the signal decreases. On further reduction in equivalence ratio, prior to lean blowout the periodicity of the time series signal is lost. This can be seen from the power spectra of time series (FFT). The power spectra of the same pressure time series is plotted by Unni and Sujith 2015. During combustion noise there is no dominant frequency and as we approach thermoacoustic instability, there is a dominant frequency of about 120 Hz. As we approach lean blowout limit, the periodicity is lost and there is no dominant frequency in the time series signal. Further, Unni and Sujith 2015 observed a slight variation in the dominant frequency as the equivalence ratio is varied which was attributed to varying flame dynamics.

4.2 Analysis of Dynamics Using Recurrence Networks

A crucial parameter in constructing the network is the recurrence threshold ε. If the threshold is very large, the network becomes very dense as there are too many links leading to false recurrences. On the other hand if the recurrence threshold is too small, the network breaks down into mutually disjointed components. Hence the network char-

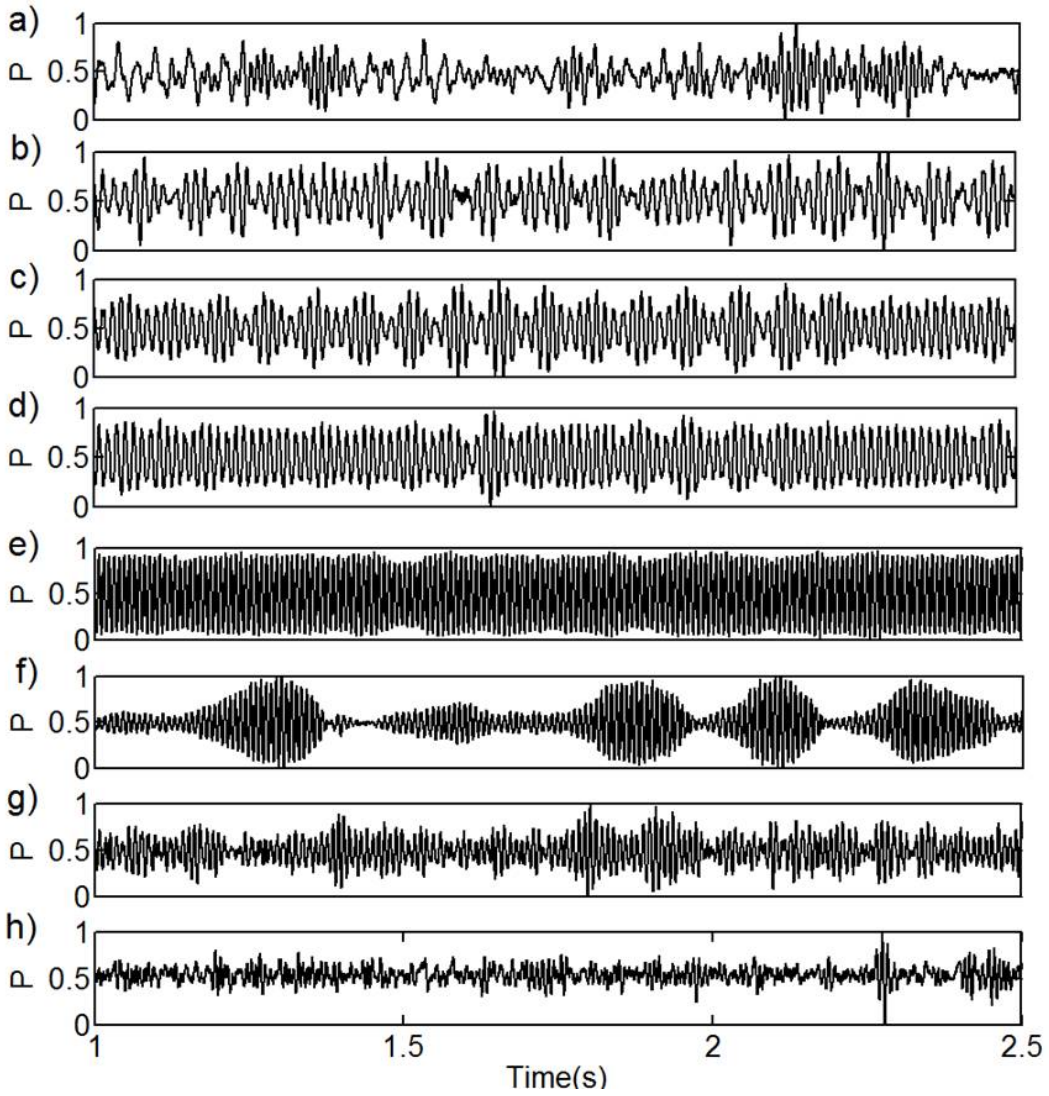

Figure 4.1: (a)-(h) The time series of the acoustic pressure (p') signal obtained from experiments at equivalence ratios, (a) 0.98, (b) 0.8, (c) 0.77, (d) 0.74, (e) 0.5, (f) 0.47, (g) 0.44, (h) 0.29 respectively.

acteristics can become ambiguous. After embedding, the size of the attractor depends on the range of the signal. The time series data is transformed into uniform deviate. Thereby, the attractor size is rescaled into the interval [0,1].

A random time series is generated and the embedding dimension is chosen to be the same as that of the time series of acoustic pressure obtained from the combustor. Recurrence networks are then constructed from the time series data of acoustic pressure and the random time series. The characteristic path length (CPL), the average of the shortest paths between two nodes, is computed for the networks constructed from time series data of acoustic pressure and from random time series. The brief description of CPL is provided in the next subsection . The CPL of RN constructed from the

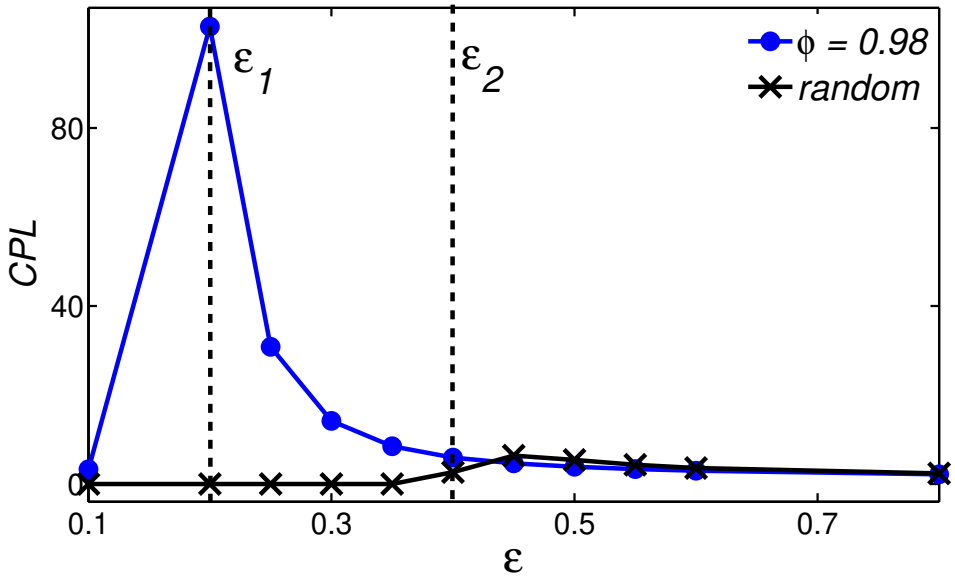

Figure 4.2: Variation of the characteristic path length (CPL) of recurrence networks with threshold, constructed from both random time series and the time series corresponding to combustion noise. The time series corresponding to combustion noise is embedded in M = 10 dimensions and the random time series is also embedded in the same dimension.

time series acquired during combustion noise decreases with increase in the threshold beyond ε_1 (Fig. 5.1). When the threshold is ε_1, then a cluster of nodes is formed. Thus, further increase in threshold results in an effective decrease in CPL as the degree of each node increases. When the recurrence threshold is greater than ε_2, the CPL of the time series corresponding to combustion noise becomes nearly the same as that of random time series. This is due to the false recurrences. Hence the upper bound and lower bound are fixed for the recurrence thresholds as $\varepsilon_1 = 0.2$ and $\varepsilon_2 = 0.4$ respectively. We use $\varepsilon = 0.25$ for our present work. Having an ε above the lower threshold ensures that the network has no disconnected nodes. Having the threshold ε below the upper threshold also ensures that RN constructed from the time series of acoustic pressure is different from the RN constructed from a random time series.

The adjacency matrix obtained from the recurrence matrix represents the topology of the network. Figure 5.3 represents the network topologies corresponding to various dynamical regimes in the turbulent combustor. The network topology is visualized using Gephi (https://gephi.org/) software. Figure 5.3(a) represents the network topology for combustion noise. Figure 5.3(b) represents the network topology for intermittency prior to thermoacoustic instability. Figure 5.3(c) represents the network topology for

thermoacoustic instability. The structure of the attractor is a limit cycle for thermoacoustic instability as the time series of acoustic pressure is periodic. Figure 5.3(d) represents the network topology for intermittency just after thermoacoustic instability. The attractor corresponding to the intermittency before thermoacoustic instability is different from that of the intermittency just after thermoacoustic instability. This is because the periodic bursts during intermittency, occurring past thermoacoustic instability are present for a longer duration in contrast to the periodic bursts during the intermittency prior to thermoacoustic instability. Figure 5.3(e) represents the network topology for the aperiodic oscillations prior to lean blowout. We can observe that the network topology resembles the geometry of the attractor. Thus, we can reaffirm that RN preserves the geometry of the attractor. Figure 5.3(f) represents the network topology for white noise. We observe that the attractors corresponding to the time series of acoustic pressure are significantly different from the attractor corresponding to white noise. We can also observe that, the nodes in the networks corresponding to that of combustion noise (Fig. 5.3(a)) and low amplitude aperiodic oscillations prior to blowout (Fig. 5.3(e)) have lower degree compared to the degree of the nodes in the networks corresponding to intermittency and thermoacoustic instability. The degree of the nodes in the network corresponding to white noise is very less compared to the RNs constructed from the time series of acoustic pressure.

4.2.1 Variation of degree distribution with recurrence threshold

We say that the degree distribution follows a power law if $P(k) = k^{-\gamma}$ where γ is the power law exponent. We study the variation of $log(P(k))$ vs $log(k)$ with the recurrence thresholds, ε = 0.2, 0.25, 0.3, 0.35 for the RNs constructed from the time series data of acoustic pressure for various dynamical states.

Figures 5.4 and 4.6 depict the variation of degree distribution of RN constructed from time series acquired during combustion noise ($\phi = 0.98$) and aperiodic oscillations prior to lean blowout ($\phi = 0.29$). We can observe that the degree distribution follows power law for the thresholds 0.2, 0.25. As the threshold increases, a significant portion of the degree distribution do not follow a power law. Theoretically, we say that there is power law, if the whole distribution follows a power law i.e., there should not be any outliers. As we are considering time series from a practical system, the entire

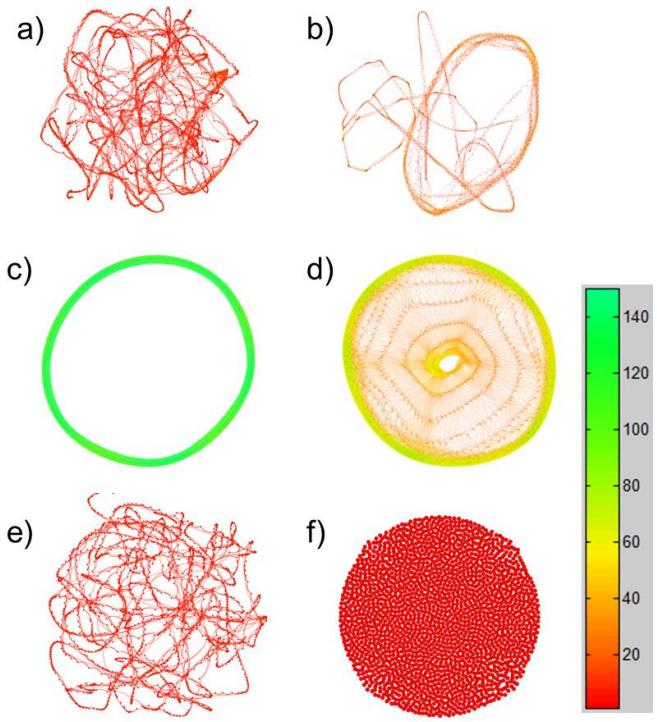

Figure 4.3: The topologies of recurrence networks constructed from the time series of acoustic pressure for the equivalence ratios (a) 0.98 (combustion noise), (b) 0.8 (intermittency prior to thermoacoustic instability), (c) 0.5 (thermoacoustic instability), (d) 0.47 (intermittency just after thermoacoustic instability), (e) 0.29 (oscillations prior to lean blowout), (f) white noise. The networks are constructed from 2000 data points and the recurrence threshold is 0.25. The colorbar shows the variation of the color with the degree of the nodes. This figure reaffirms that RN preserves the geometry of the attractor.

degree distribution may not follow a power law. We need to account for some outliers. In our present work, we consider a degree distribution to follow a power law if more than 90% of the points in the degree distribution follow a power law. Figures 7, 4.7 and 4.8 depict the variation of the degree distribution of RN constructed from the time series acquired during intermittency before thermoacoustic instability ($\phi = 0.8$), during thermoacoustic instability ($\phi = 0.5$) and during intermittency just after thermoacoustic instability ($\phi = 0.47$). We can see that the degree distribution does not follow power law for any of the chosen thresholds.

The long term distribution (invariant measure) of the phase space vectors of a dynamical system is associated with a probability distribution (Junge, 2012) of an invariant measure. The time for which a state stays at a particular location in phase space can be associated with an invariant density at that location. Thus a probability distribution can be associated with the invariant density distribution over the attractor. The degree distribution determines the local connectivity pattern of a node. As the recurrence network

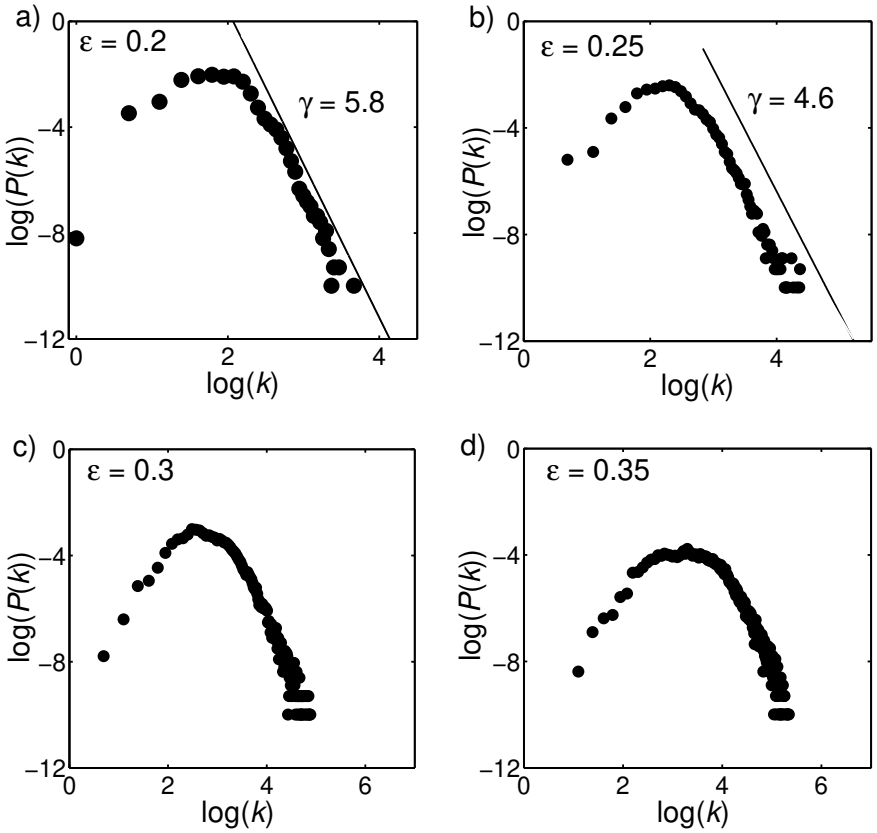

Figure 4.4: The variation of $log(P(k))$ vs $log(k)$ of recurrence networks constructed from the time series corresponding to combustion noise (ϕ = 0.98) with various thresholds ε = 0.2, 0.25, 0.3, 0.35 respectively. We can see that the power law is significant at lower thresholds.

preserves the geometry of the attractor there is a direct mapping between the degree distribution and the invariant density over the attractor (Jacob *et al.*, 2016). Therefore, the presence of power law in the degree distribution can be attributed to the presence of power law in the invariant density function. In a strict sense, if the invariant density function has a power law peak at some state X_0, i.e., of the form $f(X - X_0)^{-\lambda}$, for some $\lambda > 0$, then X_0 is a singularity. In a general case, if the invariant density function is close to power law at the state X_0, this results in power law in degree distribution. The invariant density in phase space is maximum near the singularity, hence the phase space trajectories closer to the singularity tend to converge and the recurrence rate will be more near the singularities. The nodes closer to the singularity have very high degree when compared to the nodes which are away from the singularity.

We observe that, the presence of power laws in the degree distribution of RNs corresponding to combustion noise and the oscillations prior to lean blowout is significant only at lower thresholds such as 0.2 and 0.25. This is because, the threshold corresponds

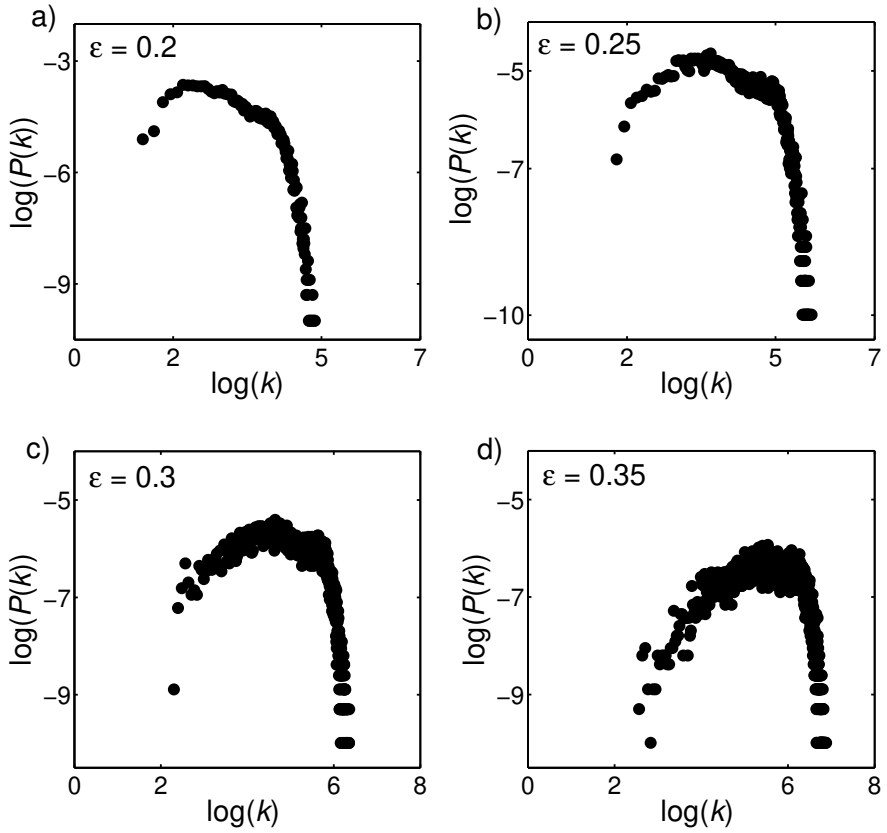

Figure 4.5: The variation of $log(P(k))$ vs $log(k)$ of recurrence networks constructed from the time series corresponding to intermittency prior to thermoacoustic instability ($\phi = 0.8$) with various thresholds $\varepsilon = 0.2, 0.25, 0.3, 0.35$ respectively. We can see that the degree distribution does not follow a power law.

to the local correlations over the reconstructed attractor in the phase space. We can state that for higher thresholds, the singularities which are local properties are masked by too many links. The invariant density changes as the recurrence threshold changes and hence the power law exponent also varies with the threshold. Further, Jacob *et al*. 2016 have reported that the recurrence networks from chaotic attractors with continuous invariant density function does not exhibit scale free topology. As there are power law degree distributions in RNs correponding to combustion noise and oscillations prior to lean blowout, we can state that the invariant density distribution over the attractors corresponding to combustion noise and the oscillations prior to lean blowout has singularities when lower thresholds such as 0.2 and 0.25 are used.

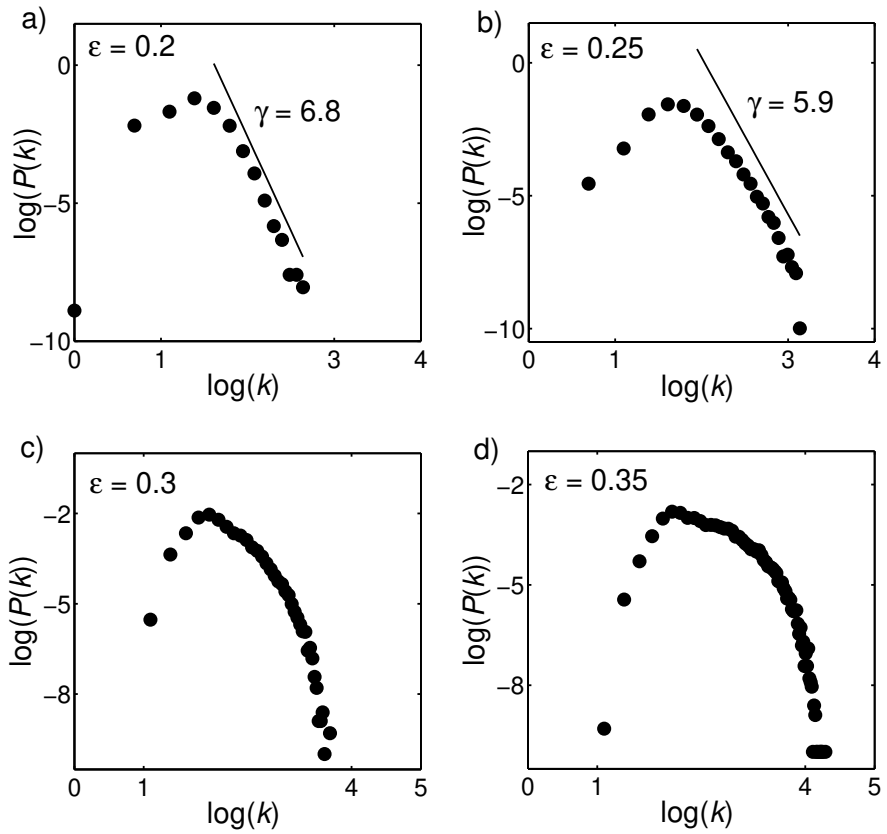

Figure 4.6: shows the variation of $log(P(k))$ vs $log(k)$ of recurrence networks constructed from the time series corresponding to low amplitude aperiodic oscillations prior to lean blowout. ($\phi = 0.29$) with various thresholds $\varepsilon = 0.2$, 0.25, 0.3, 0.35 respectively. The width of the degree distribution is less and the power law is significant for lower thresholds.

4.2.2 Variation of measures derived from RN with equivalence ratio

We proceeded to determine the impending transitions from combustion noise to lean blowout using measures such as characteristic path length and betweenness centrality derived from RN.

For the construction of RN from the time series of acoustic pressure, we consider $\varepsilon = 0.25$ for the calculation of topological measures of the network as this threshold ensures that there is a single component in the network without any disconnected nodes. The recurrence threshold ε also ensures that the RN constructed from the time series corresponding to combustion noise is different from the RN constructed from a stochastic process (white noise).

For most of the recurrence networks, the plot between $P(k)$ and k depends on the

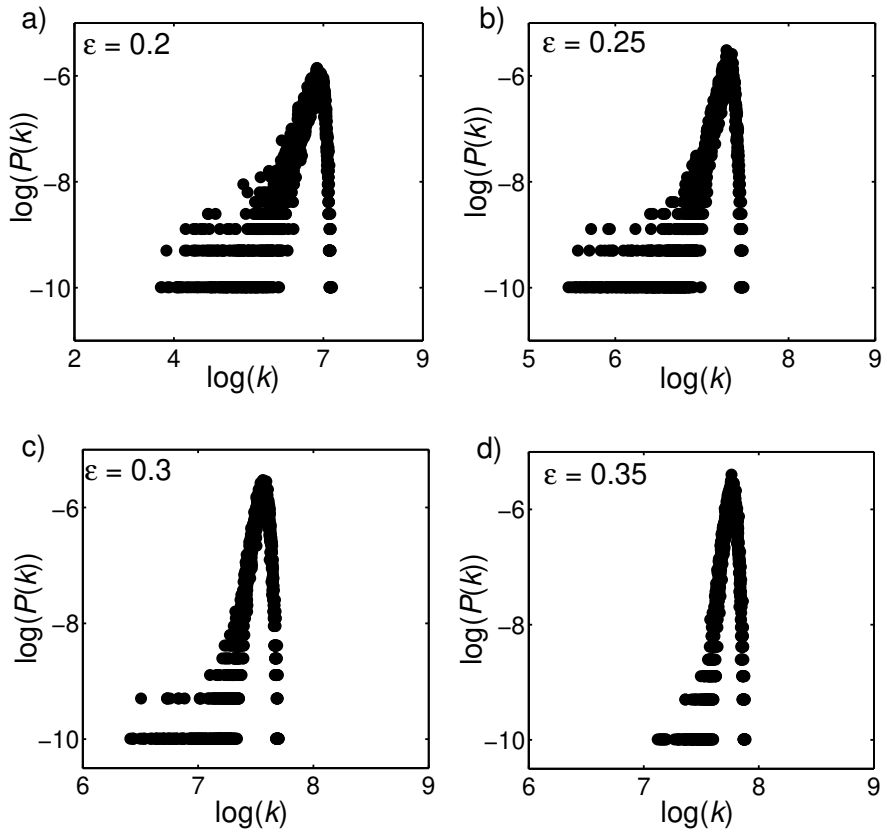

Figure 4.7: The variation of $log(P(k))$ vs $log(k)$ of recurrence networks constructed from the time series corresponding to combustion instability (ϕ = 0.5) with various thresholds ε = 0.2, 0.25, 0.3, 0.35 respectively. We can see that the degree distribution does not follow a power law.

number of data points used for the construction of RN. The degree distribution shifts to the right with increase in the number of data points (N) that are used to construct RN as the average degree increases with N. In order to avoid this dependence on N, the graph is plotted between the rescaled variables $P(k)N$ and k/N (Jacob *et al.*, 2016) for various equivalence ratios as shown in Fig. 4.9. Figure 4.9(a) to Figure 4.9(e) correspond to the degree distributions of combustion noise, intermittency prior to thermoacoustic instability, thermoacoustic instability, intermittency just after thermoacoustic instability and the oscillations prior to lean blowout respectively. Figure4.9(f) corresponds to the degree distribution in the network corresponding to white noise. In order to provide vivid variation of degree distributions corresponding to combustion noise and the oscillations prior to lean blowout, zoomed in views are plotted in Fig. 4.9(g) and Fig. 4.9(h) respectively.

As we decrease the equivalence ratio from 0.98 to 0.5, the degree distribution shifts to the right. The degree distribution of RN corresponding to thermoacoustic instability

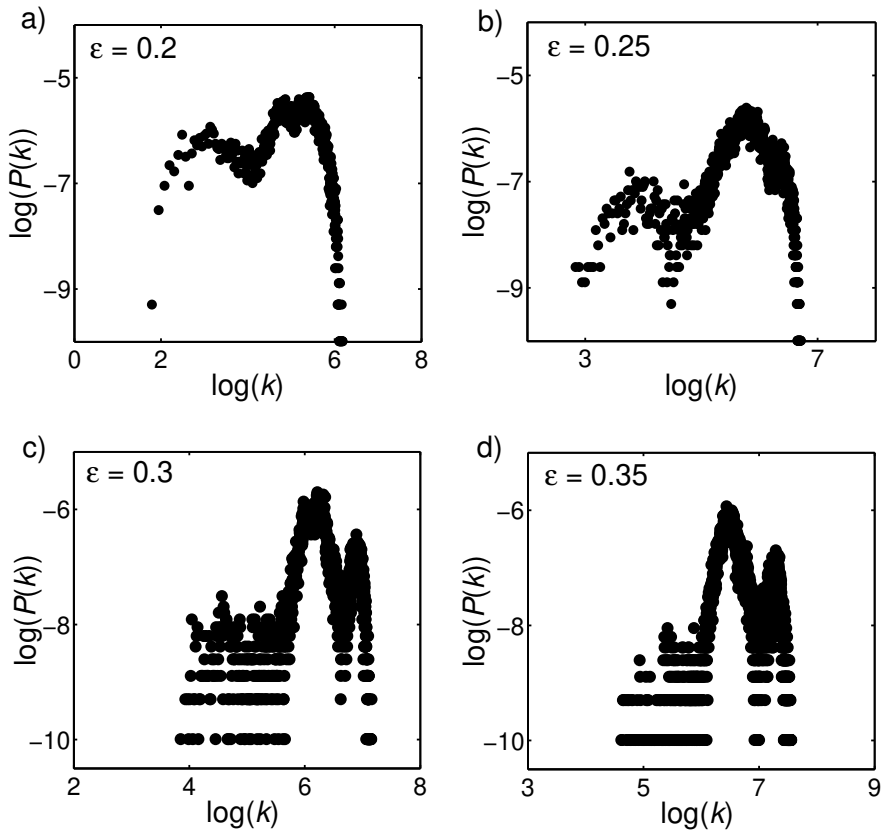

Figure 4.8: The variation of $log(P(k))$ vs $log(k)$ of recurrence networks constructed from the time series corresponding to intermittency (ϕ = 0.47) with various thresholds ε = 0.2, 0.25, 0.3, 0.35 respectively. We can see that the degree distribution does not follow a power law for these thresholds.

(Fig. 4.9(c)) is concentrated at a higher degree indicating higher connections. Hence, the phase space density at those locations is high over the attractor. We can also see in Fig. 4.9(c) that there is a single prominent peak. Such a peak in the degree distribution concentrated at higher degree corresponds to a periodic signal. This reaffirms that thermoacoustic instability is periodic. The degree distribution corresponding to ϕ = 0.47 (Fig. 4.9(d)), has multiple peaks in the degree distribution and the degree distribution is broad. Similarly, the degree distribution corresponding to the equivalence ratio ϕ = 0.8 (Fig. 4.9(b)) is also wide spread. This implies that there are large fluctuations in phase space density over the attractor. During the intermittent regime, there are large amplitude periodic fluctuations amidst the aperiodic oscillations, hence leading to the fluctuations in the local phase space density over the attractor.

We observe that the degree distribution shifts to the left, when we decrease the equivalence ratio from ϕ = 0.5 to ϕ = 0.29 and becomes more concentrated towards lower degree. This implies that the link density of RN constructed from the time se-

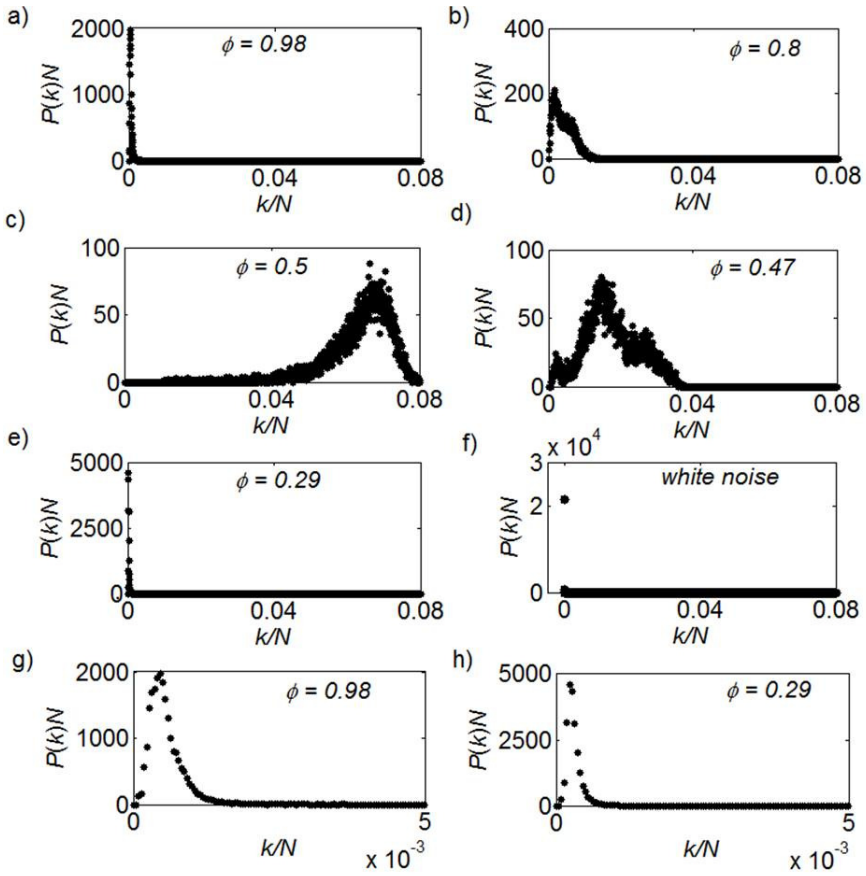

Figure 4.9: The variation of degree distribution of the RNs constructed from the time series data of acoustic pressure with equivalence ratios (a) 0.98 (combustion noise); (b) 0.8 (intermittency before thermoacoustic instability); (c) 0.5 (thermoacoustic instability); (d) 0.47 (intermittency just after thermoacoustic instability); (e) 0.29 (oscillations prior to lean blowout); and (f) white noise. There is only one point (abscissa is zero) in degree distribution corresponding to white noise as there are no connections in RN when $\varepsilon = 0.25$. The zoomed in views of the degree distributions of (g) combustion noise and (h) oscillations prior to lean blowout are shown for clear visibility of the degree distribution. We used $N = 10000$ data points and $\varepsilon = 0.25$.

ries data prior to lean blowout is less. The duration of the periodic bursts in the signal decreases as the transition occurs from thermoacoustic instability to blowout. As the recurrence rate is less, the phase space density is less which results in a shift in the degree distribution towards the left as the transition happens from thermoacoustic instability to blowout. Therefore, the recurrence rate decreases and also the average degree of the nodes decreases.

The peak in the degree distribution in the RN corresponding to the oscillations prior to lean blowout is concentrated towards lower degree than in the RN corresponding to combustion noise (Fig. 4.9). As the degree distribution can be mapped to the phase

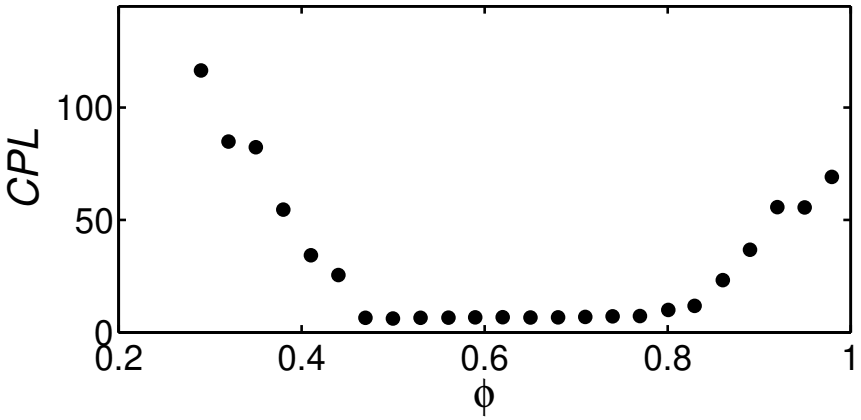

Figure 4.10: Variation of CPL with equivalence ratio. CPL is high for RN corresponding to combustion noise and decreases as we approach thermoacoustic instability. CPL again increases as we approach lean blowout limit. CPL varies with the dynamical regime. Hence CPL can be used to detect the transitions from combustion noise to thermoacoustic instability and the transitions from thermoacoustic instability to lean blowout. We used N = 5000 data points and ε = 0.25.

space density, the average density in phase space is less for the oscillations prior to lean blowout. This results in a lower degree of recurrence for the oscillations prior to blowout. We also observe that the degree of all the nodes is zero in the RN corresponding to white noise (Fig. 4.9(f)). This is because there are no connections between the nodes in the RN constructed from white noise using the threshold ε = 0.25 (Fig. 5.1).

Figure 4.10 shows the variation of CPL with equivalence ratio. CPL is minimum for the RN corresponding to thermoacoustic instability and maximum for the RN corresponding to the oscillations prior to blowout. CPL measures the spatial distance between two nodes which are nothing but two states. For a periodic signal, the recurrences in the phase space are more and hence the shortest path between two nodes is less and CPL is minimum for thermoacoustic instability. CPL is high for the oscillations prior to lean blowout and combustion noise as the average degree and the recurrence rate is less when compared with thermoacoustic instability.

Figure 4.11 shows the variation of the average betweenness centrality with equivalence ratio. We observe lower values of betweenness centrality for thermoacoustic instability and very high values for combustion noise and the oscillations prior to lean blowout. Betweenness centrality gives the information related to the presence of regions with low phase space density that separate the regions of high phase space density. High values of betweenness centrality indicate that the attractor has high local fragmentation

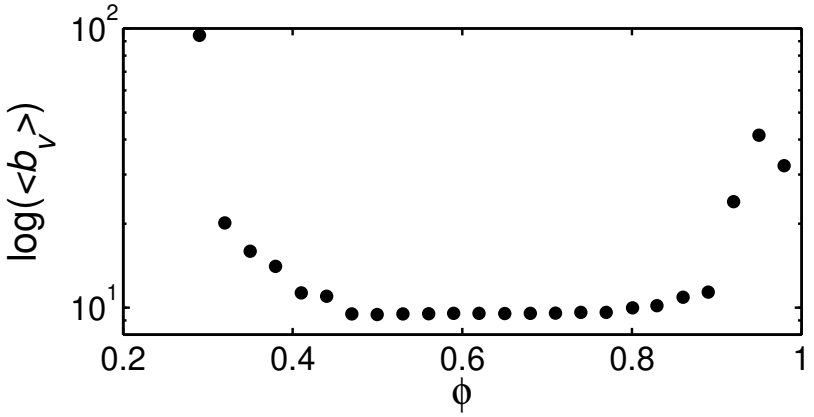

Figure 4.11: Variation of logarithmic value of average betweenness centrality in log scale with equivalence ratio. $< b_v >$ is high for the RN corresponding to combustion noise and decreases as we approach thermoacoustic instability. $< b_v >$ again increases as we approach lean blowout limit. Betweenness centrality varies with the dynamical regime and hence, can be used to detect the transition from combustion noise to thermoacoustic instability and the transition from thermoacoustic instability to lean blowout. We used N = 5000 data points and ε = 0.25.

(Donner *et al.*, 2010). As thermoacoustic instability is periodic, there will be uniform distribution of the regions with high phase space density. Hence betweenness centrality is low for thermoacoustic instability.

The network measures characteristic path length and betweenness centrality capture the transitions from combustion noise to thermoacoustic instability and from thermoacoustic instability to blowout. Hence, these measures can be used to measure the proximity to an impending transition in turbulent combustor, in industrial applications.

4.3 Conclusions

We introduce recurrence networks to study the transitions between the dynamical regimes in a combustor with turbulent reactive flow, for the first time. We observed that the network topology represents the geometry of the attractor in phase space. The network topology varies with the dynamical regimes. The network topology of RN constructed from white noise is completely different when compared with the topologies of RNs constructed from the time series of acoustic pressure for various equivalence ratios. The average degree and hence the recurrence and the degree of determinism are higher for the RNs constructed from the time series of acoustic pressure when compared with

the RN constructed from white noise. As the transition happens from combustion noise to thermoacoustic instability, the corresponding topology of the attractor changes from a complex topology to a limit cycle. During the transition from thermoacoustic instability to lean blowout, the topology of an attractor changes from a limit cycle to a complex topology. Thus, the topology of RN is different for different dynamical regimes. The plot of degree distribution in RN shows the presence of power law degree distribution in the recurrence networks constructed from the time series of acoustic pressure corresponding to combustion noise and oscillations prior to lean blowout. The presence of power law is due to the presence of singularities in the invariant density. We then proceeded to study the variation of the measures derived from RN with equivalence ratio. We observed that the variation of the network measures CPL and betweenness centrality with equivalence ratio is able to detect the transitions in a turbulent combustor and hence can be used as early warning signals. We henceforth conclude that RN can be used as a potential tool to capture the transitions between the dynamical regimes in a turbulent combustor, in industrial applications.

CHAPTER 5

STUDY OF INTERACTION BETWEEN ACOUSTIC FIELD AND UNSTEADY HEAT RELEASE RATE USING MULTIVARIATE RECURRENCE ANALYSIS

In the previous chapter, we studied the transition of a turbulent gas fired combustor operation from the state of combustion noise to thermoacoustic instability by analyzing the acoustic pressure signal using recurrence networks. However, it is the positive coupling between the acoustic field and the unsteady heat release rate fluctuations that results in the occurrence of ruinous large amplitude acoustic oscillations. Recently, many studies have been conducted to investigate the transition to such instabilities from a state of combustion noise through intermittency. As thermoacoustic instability is a result of coupled behavior between the acoustic pressure and the heat release rate, synchronization theory has been introduced to quantify the coupling between them. Pawar *et al.*2017 have found that the periodic oscillations exhibited during the state of thermoacoustic instability are of two types, namely weakly periodic and strongly periodic limit cycle oscillations. The difference between these states can be attributed to the extent of coupling that exists between the heat release rate and the acoustic oscillations in the system. Hence, it is important to characterize the synchronization transition to thermoacoustic instability in order to detect the occurrence of these dynamical states, and also the directional dependence between these oscillations. We apply measures derived from recurrence plots and recurrence networks to detect the synchronization transition observed during the onset of thermoacoustic instability. Further, we characterize the directional dependence between the acoustic field and the heat release rate fluctuations using measures derived from the cross recurrence networks constructed from their time series.

The results presented in this chapter are published in V. Godavarthi, S. A. Pawar, V. R. Unni, R. I. Sujith, N. Marwan and Jürgen Kurths, Coupled interaction between unsteady flame dynamics and acoustic field in a turbulent combustor *Vhaos: An Interdisciplinary Journal of Nonlinear Science*, 28, 113111 (2018).

5.1 Temporal Analysis of Coupled Behavior of Acoustic Field and Heat Release Rate Oscillations

The transition of the system's dynamics from a stable operation (combustion noise) to an unstable one (thermoacoustic instability) occurs when the equivalence ratio is decreased from a value close to stoichiometry to a fuel lean condition due to an increase in the mean flow velocity $\bar{u}$. In this study, the flow velocity is varied from 9.2 m/s to 18.1 m/s. The time series of p' and $\dot{q}'$ are plotted in Fig. 5.1.

When the flow velocity is 9.2 m/s, we observe low amplitude aperiodic oscillations in both p' and $\dot{q}'$ (Fig. 5.1(a)). This state is called combustion noise. We observe that p' and $\dot{q}'$ oscillate independently during this state. As $\bar{u}$ increases from 9.2 m/s to 11.9 m/s, we observe a transition from combustion noise to intermittency. During intermittency, there are bursts of periodic oscillations occuring at random intervals amidst epochs of aperiodic oscillations (Fig. 5.1(b). We find that p' and $\dot{q}'$ appear to be locked during the bursts of periodic oscillations and they appear to oscillate independently during the aperiodic epochs of oscillations. When $\bar{u}$ increases to 12.5 m/s, we observe the occurrence of weakly periodic LCO (Fig. 5.1(c)). During this state, there is a wide variation in the cycle-to-cycle amplitude of both the signals, while their phases appear to be locked in time. A further increase in $\bar{u}$ to 16.2 m/s leads to a transition from this weakly periodic LCO to a strongly periodic LCO (Fig. 5.1(d)). During this state, both the phases as well as the amplitudes appear to be highly correlated in time.

Pawar *et al.* 2017 used a measure of synchronization based on the recurrence behavior of the phase space trajectory of the signal, i.e., the plot of probability of recurrence $P(\tau)$, to characterize the type of synchronization observed during the regimes shown in Fig. 5.1. They found that the signals are desynchronized during the state of combustion noise (Fig. 5.1(a)). They described intermittency as the state of intermittent phase synchronization (IPS) where during the bursts of periodic oscillations, both signals are phase locked and during the aperiodic epochs, the signals are desynchronized. They reported that during the state of weakly periodic LCO, the signals are phase synchronized (PS) and during the state of strongly periodic LCO, the signals are in a state of generalized synchronization (GS).

Further, we note that the construction of $P(\tau)$ plots is based on characterizing the

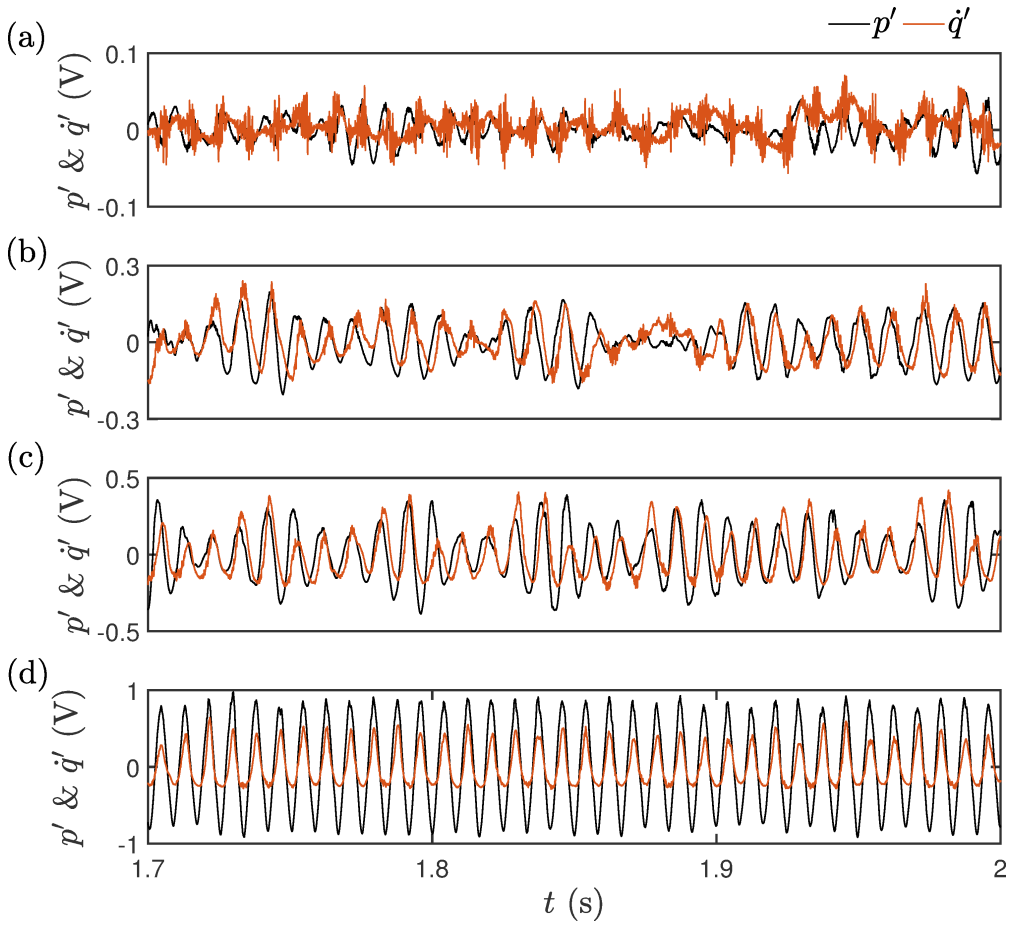

Figure 5.1: (a)-(d) The time series of acoustic pressure fluctuations (p') shown in black and unsteady heat release rate fluctuations ($\dot{q}'$) shown in red at mean flow velocities $\bar{u}$ = 9.2, 11.9, 12.5 and 17.2 m/s, respectively.

recurrences in the phase space trajectories of the signal. Therefore, in order to analyze the coupled behavior of p' and $\dot{q}'$ signals, we plot recurrence plots obtained from JRM and CRM of these signals (shown in Fig. 5.2).

5.1.1 Analysis of synchronization transition using multivariate recurrence plots

A black dot in JRP (Figs. 5.2(a-d)) represents the presence of simultaneous recurrence in both signals. During the desynchronized state, we observe irregular points in the JRP (Fig. 5.2(a)) as the time series of both p' and $\dot{q}'$ are aperiodic. The density of the black dots is low during the desynchronized state due to the lower occurrence of simultaneous recurrences in p' and $\dot{q}'$. During the IPS state, we observe discontinuous diagonal lines and irregular black patches(Fig. 5.2(b)). This is due to the presence of both weakly periodic oscillations during the epochs of bursts and low amplitude aperiodic regimes in

p' and $\dot{q}'$, respectively. The presence of discontinuous diagonal lines in Fig. 5.2(c) is due to the weakly periodic nature of LCO observed during the PS state. During the GS state, as the signals exhibit strongly periodic LCO and as they share a functional relationship (Pawar *et al.*, 2017), there are more occurrences of simultaneous recurrences. Hence, we observe lines parallel to the main diagonal line (Fig. 5.2(d)). From the JRP, we find that the occurrence of simultaneous recurrences in p' and $\dot{q}'$ increases with the onset of synchronization between p' and $\dot{q}'$.

Figures 5.2(e-h) show the CRPs of p' and $\dot{q}'$. The cross recurrence rate chosen (0.05) is lower than the individual recurrence rates (0.08) in order to distinguish the individual recurrence networks (Feldhoff *et al.*, 2012). CRP encodes the information related to the presence of similar states in the phase space of the signals. During GS, there are similar states in both the signals and hence the CRP (Fig. 5.2(h)) looks similar to the JRP (Fig. 5.2(d)). During the desynchronized state, the CRP is completely different from the individual RPs of p' and $\dot{q}'$, as the structures present in CRP are different from that of JRP. The occurrence of similar states is seen when there is synchronization between the states. The appearance of these JRPs and CRPs in Fig. 5.2 is specific to our system in which we observe synchronization transition from an aperiodic state to a periodic state. These plots will appear differently for other systems where the synchronized state is not a periodic one.

RP is a graphical tool for visualizing the dynamics of complex systems. The qualitative visual description of such plots can be quantified using measures from recurrence quantification analysis (RQA) (Webber and Zbilut, 1994; Marwan *et al.*, 2002) as given in the previous chapter. This quantification gives more objective results than a visual description. The plots of these measures are shown in Fig. 5.3.

Figure 5.3(a) shows the variation of DET_J (eq.2.9) computed from the JRP of p' and $\dot{q}'$ with $\bar{u}$. We observe that DET_J becomes maximum and reaches a value closer to 1 during the occurrence of PS, as the signals observed during this state are weakly periodic. Thus, DET_J can be used to detect the PS state in this case as we observe periodic dynamics during the PS state. Figure 5.3(b) depicts the variation of RR of the joint recurrence matrix with $\bar{u}$. We observe that RR_J (eq. 2.13) increases with $\bar{u}$. Due to the onset of synchronization, the simultaneous occurrence of recurrences in JRPs increases which leads to the increase in RR_J. We observe that RR_J is maximum

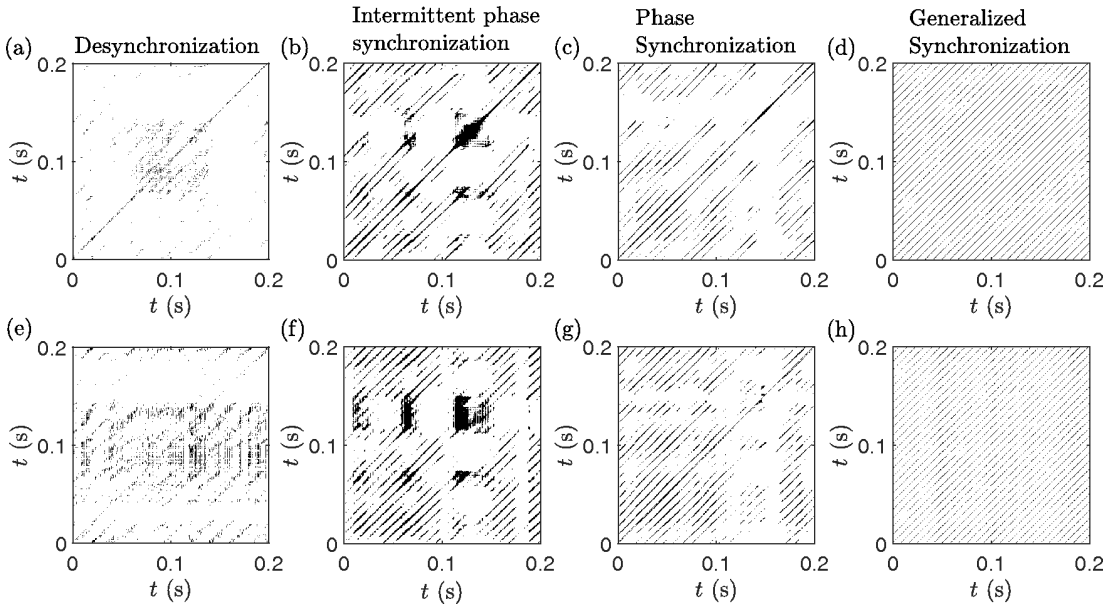

Figure 5.2: (a)-(d) Joint recurrence plots (JRP) of p' and $\dot{q}'$, and (e)-(h) Cross recurrence plots (CRP) of p' and $\dot{q}'$ for desynchronized, IPS, PS and GS states, respectively. An embedding dimension of 6, a time delay of 2 ms and a fixed recurrence rate of 0.08 is used for the computation of individual recurrence matrices and a fixed recurrence rate of 0.05 is used for the computation of cross recurrence matrix.

during GS and is also able to detect the transition from desynchronized state to PS. The transition to PS state happens via IPS state which results in the smooth change in RR_J. RR_J displays a plateau in the plot during the region of PS in the system dynamics. This further indicates that the recurrence properties of both signals nearly remain the same, although the flow velocities are sufficiently increased during this state. During the transition from PS to GS, as the diagonal lines in JRP becomes more continuous (Fig. 5.2(d)) due to the increase in recurrence behavior of trajectories, their mean RR_J values exhibit an increase in the plot (Fig. 5.3(b)).

Figure 5.3(c) depicts the variation in CPR (eq. 2.11) and JPR (eq. 2.12) computed from the $P(\tau)$ plots of p' and $\dot{q}'$. We observe that the means of both CPR and JPR increase with increase in $\bar{u}$. During the PS state, as the location of peaks in $P(\tau)$ plots of the two signals match (Pawar *et al.*, 2017), CPR becomes closer to 1. Hence it can be used to detect the PS state. We also observe that CPR shows a slight change during the transition to GS. On the other hand, we observe that JPR reaches its maximum during GS and also is able to detect the transition from PS to GS state. The presence of IPS between the desynchronized state and the PS state results in the smooth change of these measures.

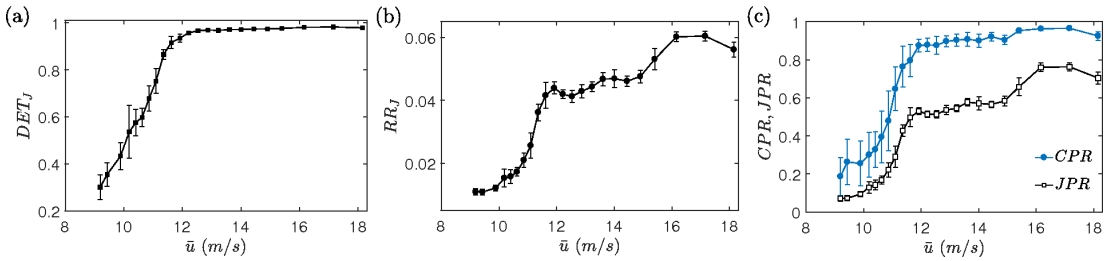

Figure 5.3: (a)-(c) Variation of DET_J, RR_J, CPR and JPR with $\bar{u}$, respectively. The properties are computed for embedding dimension of 6, a time delay of 2 ms and a fixed RR of 0.08. The signal of length 30000 is divided into windows of length 3000 and the mean values of the properties are plotted. The error bars represent the standard deviation.

We find that the measures computed using the recurrence plots and the $P(\tau)$ plots show the transition from desynchronized state to PS and GS states, and hence, can be used as indices to detect the PS and GS states in thermoacoustic systems.

5.1.2 Detection of synchronization transition and directional dependence using recurrence networks

Now, we aim to detect the directionality of coupling that exists between p' and $\dot{q}'$ during different dynamical states. We construct joint and intersystem recurrence networks and compute network properties for this purpose.

Figures 5.4(a-d) are the JRN of p' and $\dot{q}'$ obtained during different states of combustion dynamics. The nodes are colored based on their degree and the colorbar to the right indicates the variation of color with the degree of the node. We uncover that as the transition occurs from the desynchronized state (Fig. 5.4(a)) to GS state (Fig. 5.4(d)), the degree distribution becomes more uniform and concentrated towards lower degree (shown by blue color). During desynchronized state (Fig. 5.4(a)), the color of the nodes varies from blue (lower degree) to red (higher degree). During the GS state in Fig. 5.4(d), the color of the nodes is almost the same and concentrated towards lower degree. The topology is similar to a limit cycle. This is a result of the occurrence of more simultaneous recurrences and the periodic nature of the signals during the GS state. During the IPS state (Fig. 5.4(b)), we observe that some part of the topology is similar to a limit cycle, whereas some part is similar to a chaotic structure. During bursts of periodic oscillations, the signals are phase synchronized and hence have

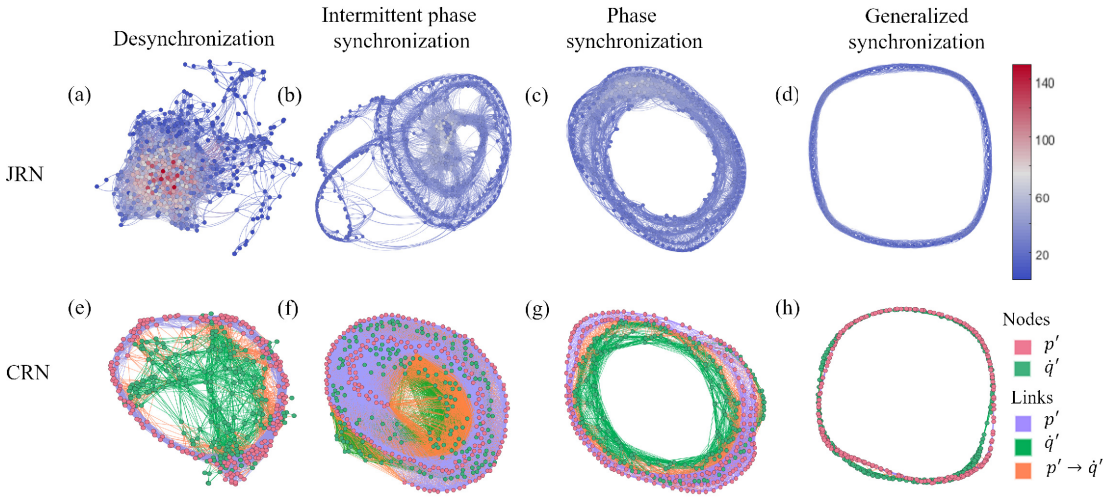

Figure 5.4: (a)-(d) Topologies of the joint recurrence networks (JRN) constructed from the joint recurrence matrices and (e)-(h) topologies of the networks constructed from the intersystem recurrence networks with the interlinks based on the cross recurrence matrices (CRN) during desynchronized, IPS, PS and GS states, respectively. The networks are constructed for 5000 data points with a fixed recurrence rate of 0.08 for individual recurrence matrices and 0.05 for the cross recurrence matrices. For the purpose of clear visualization, 500 nodes are considered for JRN and 200 nodes for each individual network in CRN. We use Force Atlas layout in Gephi software (`https://gephi.org/`) for network visualization.

simultaneous occurrence of recurrences and periodic dynamics. During the aperiodic regions, the signals are desynchornized and we observe a chaotic structure in the network. We observe from Figs. 5.4(c-d) that during the PS state, the limit cycle is wider when compared with the GS state. This is due to the weakly periodic oscillations exhibited during the PS state and the strongly periodic oscillations observed during the GS state.

Figures 5.4(e-h) show the network topologies of the individual recurrence networks of p' and $\dot{q}'$ along with the connections between them obtained for different states of combustion dynamics. The links with the orange color indicate the interconnections between the p' and $\dot{q}'$ networks obtained from the CRM computed using the Euclidean distance measured from the states in the phase space of p' to the states in the phase space of $\dot{q}'$ ($p' \rightarrow \dot{q}'$). The interlink represents the presence of a state in the same neighborhood of both the phase spaces, i.e., the interlink connects the nodes which correspond to the states that are similar to both p' and $\dot{q}'$.

During the desynchronized state (Fig. 5.4(e)), the networks of p' and $\dot{q}'$ are connected in an irregular fashion and the individual networks do not overlap. This is due

to the presence of very few similar states. During the IPS state (Fig. 5.4(f)), some nodes of both networks (red and green color) in some regions are closer, while some are farther apart. This is due to the phase locking behavior of both the signals during the bursts which results in the presence of similar states and the desynchronous behavior in the aperiodic parts of the signal. During the PS state (Fig. 5.4(g)), we observe that the individual networks and the inter connections form a wider limit cycle, whereas the width of this topology becomes less during the GS state (Fig. 5.4(f)) and hence, the individual networks appear much closer to each other. The proximity and overlap between the individual networks observed during the GS state indicate the presence of similar states.

We use a network measure, transitivity obtained from both joint and intersystem recurrence matrices to quantify the synchronization transition in the system. Figure 5.5(a) shows the variation of joint transitivity ($\mathcal{T}_J$ - blue color) (eq. 2.15) and transitivity ratio ($Q_{\mathcal{T}}$- red color) (eq. 2.16) with $\bar{u}$. $\mathcal{T}_J$ increases with $\bar{u}$ and reaches its maximum value during the GS state. Due to the presence of similar states during GS, the individual transitivities will be similar to that of $\mathcal{T}_J$. Thus the normalized measure, $Q_{\mathcal{T}}$ reaches a maximum value around 1 during GS. Hence, $Q_{\mathcal{T}}$ can be used as an index to detect the GS state and both the measures, $\mathcal{T}_J$ and $Q_{\mathcal{T}}$, can be used to detect the synchronization transition. The smooth increase in these measures from the desynchronized state to PS is due to presence of the IPS state.

Figure 5.5(b) shows the variation in cross transitivities $\mathcal{T}_{p'\dot{q}'}$, $\mathcal{T}_{\dot{q}'p'}$ with $\bar{u}$. $\mathcal{T}_{p'\dot{q}'}$ is the probability that two nodes in the recurrence network of $\dot{q}'$ are connected given that they are neighbors to a node in the recurrence network of p'. The interconnections between p' and $\dot{q}'$ are identified using the CRP from $p' \rightarrow \dot{q}'$. As the CRM is not necessarily symmetric, the interconnections can differ based on whether the distance matrix is computed from $p' \rightarrow \dot{q}'$ or from $\dot{q}' \rightarrow p'$. Due to the differences in the interconnections, the cross transitivity need not be symmetric and hence can be used as an indicator of directionality between the signals of coupled oscillators. The differences in the cross transitivity can be due to the way in which the individual systems are coupled (Feldhoff *et al.*, 2012). We observe that during the states of desynchronization and IPS, both $\mathcal{T}_{p'\dot{q}'}$ and $\mathcal{T}_{\dot{q}'p'}$ have nearly the same value, as the coupling between p' and $\dot{q}'$ is weak. During the PS state, we observe that $\mathcal{T}_{p'\dot{q}'}$ is higher than $\mathcal{T}_{\dot{q}'p'}$, which might happen due to a stronger influence of $\dot{q}'$ on p' than vice versa. We know that there is a mutual coupling

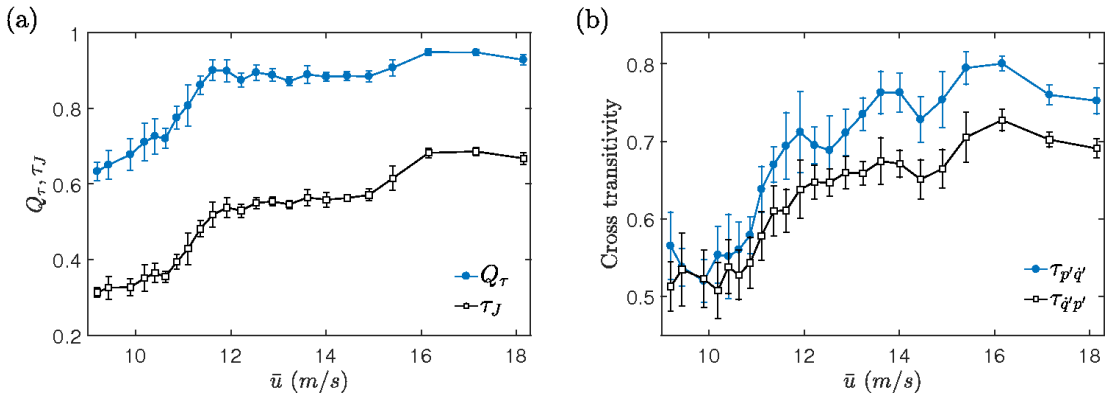

Figure 5.5: (a) Variation of joint transitivity ($\mathcal{T}_J$) and transitivity ratio ($Q_\mathcal{T}$) of joint recurrence networks with $\bar{u}$. (b) Variation of cross transitivities ($\mathcal{T}_{p'\dot{q}'}, \mathcal{T}_{\dot{q}'p'}$) of the cross recurrence networks with $\bar{u}$. The networks are constructed using 5000 data points using an embedding dimension of 6, time delay of 2 ms and a fixed RR of 0.08 for the individual recurrence networks and 0.05 for the cross recurrence networks. The signal of length 30000 is divided into windows of length 3000, and the mean values of the properties are plotted. The error bars represent the standard deviation.

between p' and $\dot{q}'$ during the state of thermoacoustic instability. Thus, the difference between $\mathcal{T}_{p'\dot{q}'}$ and $\mathcal{T}_{\dot{q}'p'}$ observed in Fig. 5.5(b) may be due to an asymmetrical bidirectional coupling between p' and $\dot{q}'$ with stronger influence of $\dot{q}'$ on p' than vice versa. In most systems which undergo synchronization transition, we don't see a growth in amplitude like in our case (Balanov *et al.*, 2008). This results in a speculation that the dynamics observed in our system can be due to parametric resonance, and need not be synchronization. However, if the dynamics were a result of resonance, there should not be any asymmetry in the coupling between p' and $\dot{q}'$, which we discovered in our system. This reaffirms that the transition to thermoacoustic instability is indeed due to the synchronization between p' and $\dot{q}'$.

5.2 Conclusions

We quantified the synchronization transition of the acoustic pressure (p') and the unsteady heat release rate ($\dot{q}'$) fluctuations in a thermoacoustic system using measures derived from multivariate recurrence plots and recurrence networks. Further, we demonstrated that the measures, determinism (DET) and correlation of probability of recurrence (CPR), can be used to detect the occurrence of the state of phase synchronization (PS) and the measures, recurrence rate (RR) and joint probability of recurrence (JPR),

can be used to detect the occurrence of generalized synchronization state (GS). We constructed the joint recurrence networks and the cross recurrence networks from the corresponding time series and found that the network properties, namely joint transitivity ($\mathcal{T}_J$) and transitivity ratio ($Q_{\mathcal{T}}$), are efficient indices to detect GS. Further, in order to characterize the directionality of coupling between p' and $\dot{q}'$, we used cross transitivity. We discovered a possible asymmetric bidirectional coupling between p' and $\dot{q}'$ during the PS and GS states. We observed that $\dot{q}'$ exerts greater influence on p' than vice versa. This directional dependence will be crucial in designing effective control mechanisms and modelling the system behavior during thermoacoustic instability. In our system, as we observed that heat release rate has stronger influence on acoustic pressure, a control on the flame might possibly be more efficient than a control on the acoustic field in order to prevent thermoacoustic instability.

CHAPTER 6

CONCLUSIONS AND SCOPE FOR FUTURE WORK

The main focus of this thesis is to investigate the transitions in a turbulent combustor using recurrence networks. Firstly, we looked at the transition from combustion noise to thermoacoustic instability and lean blowout using recurrence network analysis. We established that the thermoacoustic system at hand is a complex system. Complex networks are used to study complex systems to quantify the collective beahivor exhibited by the system. Since, the time series of the unsteady pressure is a reflection of the spatio temporal dynamics of the system, we constructed complex networks from the acoustic time series acquired from a bluff body stabilized turbulent combustor. In order to understand the dynamics, we constructed recurrence networks which is based on a fundamental property of deterministic dynamical system, recurrence. We chose an optimum threshold using the behavior of network properties on the threhold. We reaffirmed that RNs preserve the geometry of the attractor and hence ar capable of capturing the transitions occuring in a turbulent combustor. We also observed the presence of power law degree distributions during combustion noise and the oscillations prior to lean blowout which encode information about the presence of singularities in the attractor. We also demonstrated that the network properties such as characteristic path length and betweenness centrality can capture the transitions much ahead and hence can be used a early warning measures to forewarn thermoacoustic instability and lean blowout. All in all, we showed that recurrence networks can be used as a potential tool to study transitions in a turbulent combustor.

Since, thermoacoustic instability in the system involving turbulent flow is associated with a synchronization phenomenon of two mutually coupled non-identical oscillators viz., the acoustic field in the confinement and the turbulent reactive flow present in the system. Since, we established that recurrence networks are a useful tool to analyze the transitions, we extend recurrence analysis to bivarate recurrence analysis to analyze the coupled behavior of the acoustic pressure and unsteady flame dynamics in a turbulent combustor. We constructed joint and cross recurrence matrices and used quanitifiers

such as joint recurrence rate, determinism and some of the measures from probability of recurrence plots such as correlation of probability of recurrence and joint probabilty of recurrence are able to detect the onset of the PS and GS states. Further, we constructed joint recurrence and inter-system recurrence networks. We observe that that the network topologies are similar during GS state and different phase spaces during the desynchronized state. We quantified the topologies using joint transitivity and a normalized measure transitivity ratio to detect the onset of GS.

As we are studying the tranistion to thermoacoustic instability as an interaction between two oscillators, acoustic field and the turbulent reactive flow, it is very important to identify the directional dependence between them. We used the asymmetry in the cross recurrence networks and computed cross transitivity to identify the directionality. We discovered an asymmetric bidirectional coupling between the acoustic field and the unsteady flame dynamics with the turbulent reactive flow where the turbulent reactive flow affects the acoutic field more than vice versa.

Scope for Future Work

The present thesis established the recurrence network framework to investigate the complexity or the dynamical features of the thermoacoustic systems by obtaining the complex networks from the time series data using recurrence condition. The directional dependence is also detected between the acoustic field and the turbulent reactive flow using temporal analysis. We attempt to model the spatio-temporal dynamics using synchronization between network of oscillators representing the hydrodynamics, combustion and acoustics using the directional dependence discovered. A simple numerical model will aid in demonstrating that synchonization is a major reason for observing the complex dynamics and also allows us to perform numerical experiments to disrupt synchronization.

Further, we studied the interaction between acoustic field and turbulent reactive flow in a turbulent combustors using bivariate recurrence networks. This framework is applied to mutual synchronization and can be extended to forced synchonization of thermoacoustic system as well which will be helpful in developing open loop control strategies. Analyzing the forcing, acoustic field and the heat release rate using multiplex

recurrence network can pave way to enable effective forcing strategies by identifying the mutual directional dependence between these oscillators.

APPENDIX A

ACOUSTIC FIELD AND UNSTEADY HEAT RELEASE RATE FLUCTUATIONS IN A TURBULENT COMBUSTOR ARE SELF-SUSTAINED OSCILLATORS

In this chapter, we establish acoustic field and unsteady heat release rate fluctuations in a turbulent combustor as self-sustained oscillators to be able to apply synchronization framework to thermoacoustic system.

In order to prove that the acoustic field in a duct with turbulent flow is a self-sustained oscillator, we perform separate experiments on the same experimental setup (used in the present study) in the cold flow environment by removing the flame and maintaining the same flow conditions. Figures 6a, b show the time series and the amplitude spectrum of the pressure signal acquired for the air flow condition of 9.1 m/s, respectively. We observe a dominant peak at 733 Hz, compared to the other low magnitude frequency peaks in the spectrum (Fig. 6b). Further, the existence of a dominant frequency in the spectrum indicates the presence of correlations in the signal, which is different from the characteristics of noise. This affirms that for turbulent flows confined in a duct, from the viewpoint of oscillation theory, acoustic pressure is a self-sustained oscillator with seemingly chaotic fluctuations.

The results presented in this chapter are published in V. Godavarthi, S. A. Pawar, V. R. Unni, R. I. Sujith, N. Marwan and Jürgen Kurths, Coupled interaction between unsteady flame dynamics and acoustic field in a turbulent combustor *Chaos: An Interdisciplinary Journal of Nonlinear Science*, 28, 113111 (2018).

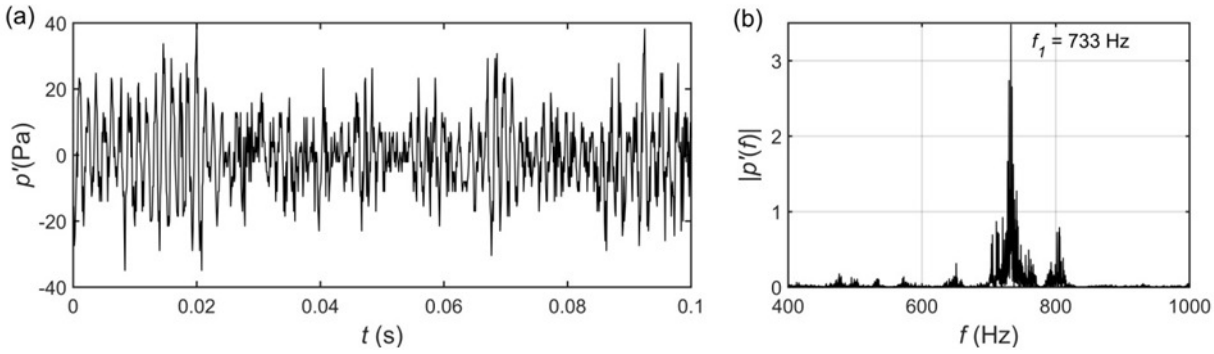

Figure A.1: (a), (b) The time series and the amplitude spectrum of the acoustic pressure signal acquired during the cold conditions with the air flow velocity of 9.1 m/s, respectively. In the presence of a turbulent flow, the amplitude spectrum shows a sharp peak at $f_1 = 733$ Hz, which is an indicative of correlated self-sustained oscillations in the signal.

Further, various studies have been conducted on open turbulent flames in the past. Turbulent flows cause oscillations in the flame front, that in turn, cause fluctuations in the flame surface area, and hence, fluctuations in the heat release rate. Several studies showed that sound pressure levels (SPL) of combustion noise produced by open turbulent jet flames exhibits a broadband spectrum concentrated at lower frequencies (Shivashankara *et al.*, 1973; Strahle, 1977; Strahle and Jagoda, 1989; Rajaram and Lieuwen, 2009). Thus, uncoupled turbulent flames with the acoustic field can behave like a self-sustained oscillator with aperiodic fluctuations.

Thus, under the influence of a turbulent flow, the acoustic field and the heat release rate in the combustor can be considered as self-sustained aperiodic oscillators. Each of these oscillators are otherwise damped oscillators; however, the presence of continuous perturbations from the inherent turbulent hydrodynamic flow makes them self-sustained oscillators. Thus, synchronization framework can be applied to study the onset of thermoacoustic instability in a turbulent combustor.

Further, in the combustor, these oscillators are not distinct but are inherently coupled with each other through the medium of turbulent flow field. Similar behavior can be seen in complex biological systems such as human respiratory system, where synchronization between cardiovascular and respiratory systems is considered even though these subsystems cannot be considered as independent(Schäfer *et al.*, 1999). This is because a weak coupling between these systems is observed and it also has been reported that these systems are generally not phase-locked. Analogously, in a complex

system such as ours, during combustion noise, the acoustic pressure and unsteady heat release rate are desynchronized. This desynchronized behavior can be due to the weak coupling between the turbulent reactive flows and the combustor acoustics. During the transition to thermoacoustic instability, the coupling between these subsystems gradually enhances, leading to a generalized synchronization state.

REFERENCES

1. **Balanov, A.**, **N. Janson**, **D. Postnov**, and **O. Sosnovtseva**, *Synchronization: from simple to complex*. Springer Science & Business Media, 2008.

2. **Bar-Yam, Y.**, *Dynamics of complex systems*, volume 213. Addison-Wesley Reading, MA, 1997.

3. **Barabási, A.-L.** (2011). The network takeover. *Nature Physics*, **8**(1), 14.

4. **Barabási, A.-L.** and **R. Albert** (1999). Emergence of scaling in random networks. *science*, **286**(5439), 509–512.

5. **Barabási, A.-L.** and **E. Bonabeau** (2003). Scale-free networks. *Scientific american*, **288**(5), 60–69.

6. **Boccaletti, S.**, **V. Latora**, **Y. Moreno**, **M. Chavez**, and **D.-U. Hwang** (2006). Complex networks: Structure and dynamics. *Physics reports*, **424**(4-5), 175–308.

7. **Broda, J.**, **S. Seo**, **R. Santoro**, **G. Shirhattikar**, and **V. . Yang**, An experimental study of combustion dynamics of a premixed swirl injector. *In Symposium (International) on Combustion*, volume 27. Elsevier, 1998.

8. **Cao, L.** (1997). Practical method for determining the minimum embedding dimension of a scalar time series. *Physica D: Nonlinear Phenomena*, **110**(1-2), 43–50.

9. **Chakravarthy, S.**, **R. Sivakumar**, and **O. Shreenivasan** (2007). Vortex-acoustic lock-on in bluff-body and backward-facing step combustors. *Sadhana*, **32**(1), 145–154.

10. **Charakopoulos, A.**, **T. Karakasidis**, **P. Papanicolaou**, and **A. Liakopoulos** (2014). The application of complex network time series analysis in turbulent heated jets. *Chaos: An Interdisciplinary Journal of Nonlinear Science*, **24**(2), 024408.

11. **Chiocchini, S.**, **T. Pagliaroli**, **R. Camussi**, and **E. Giacomazzi** (2017). Chaotic and linear statistics analysis in thermoacoustic instability detection. *Journal of Propulsion and Power*, **34**(1), 15–26.

12. **Correa, S. M.** (1993). A review of nox formation under gas-turbine combustion conditions. *Combustion science and technology*, **87**(1-6), 329–362.

13. **Crocco, L.** and **S.-I. Cheng** (1956). Theory of combustion instability in liquid propellant rocket motors. Technical report, PRINCETON UNIV NJ.

14. **Culick, F.** (1994). Some recent results for nonlinear acoustics in combustion chambers. *AIAA journal*, **32**(1), 146–169.

15. **Domen, S.**, **H. Gotoda**, **T. Kuriyama**, **Y. Okuno**, and **S. Tachibana** (2015). Detection and prevention of blowout in a lean premixed gas-turbine model combustor using the concept of dynamical system theory. *Proceedings of the Combustion Institute*, **35**(3), 3245–3253.

16. **Donges, J. F.**, **R. V. Donner**, **M. H. Trauth**, **N. Marwan**, **H.-J. Schellnhuber**, and **J. Kurths** (2011). Nonlinear detection of paleoclimate-variability transitions possibly related to human evolution. *Proceedings of the National Academy of Sciences*, **108**(51), 20422–20427.

17. **Donner, R. V.**, **M. Small**, **J. F. Donges**, **N. Marwan**, **Y. Zou**, **R. Xiang**, and **J. Kurths** (2011). Recurrence-based time series analysis by means of complex network methods. *International Journal of Bifurcation and Chaos*, **21**(04), 1019–1046.

18. **Donner, R. V.**, **Y. Zou**, **J. F. Donges**, **N. Marwan**, and **J. Kurths** (2010). Recurrence networksâĂŤa novel paradigm for nonlinear time series analysis. *New Journal of Physics*, **12**(3), 033025.

19. **Eckmann, J.**, **S. O. Kamphorst**, **D. Ruelle**, *et al.* (1995). Recurrence plots of dynamical systems. *World Scientific Series on Nonlinear Science Series A*, **16**, 441–446.

20. **Feldhoff, J.**, **R. V. Donner**, **J. F. Donges**, **N. Marwan**, and **J. Kurths** (2013). Geometric signature of complex synchronisation scenarios. *EPL (Europhysics Letters)*, **102**(3), 30007.

21. **Feldhoff, J. H.**, **R. V. Donner**, **J. F. Donges**, **N. Marwan**, and **J. Kurths** (2012). Geometric detection of coupling directions by means of inter-system recurrence networks. *Physics Letters A*, **376**(46), 3504–3513.

22. **Fichera, A.**, **C. Losenno**, and **A. Pagano** (2001). Experimental analysis of thermoacoustic combustion instability. *Applied Energy*, **70**(2), 179–191.

23. **Gao, Z.** and **N. Jin** (2009). Flow-pattern identification and nonlinear dynamics of gas-liquid two-phase flow in complex networks. *Physical Review E*, **79**(6), 066303.

24. **Gao, Z.-K.**, **N.-D. Jin**, **W.-X. Wang**, and **Y.-C. Lai** (2010). Motif distributions in phase-space networks for characterizing experimental two-phase flow patterns with chaotic features. *Physical Review E*, **82**(1), 016210.

25. **Goh, C. S.** and **A. S. Morgans** (2013). The influence of entropy waves on the thermoacoustic stability of a model combustor. *Combustion Science and Technology*, **185**(2), 249–268.

26. **Goswami, B.**, **G. Ambika**, **N. Marwan**, and **J. Kurths** (2012). On interrelations of recurrences and connectivity trends between stock indices. *Physica A: Statistical Mechanics and its Applications*, **391**(18), 4364–4376.

27. **Gotoda, H.**, **M. Amano**, **T. Miyano**, **T. Ikawa**, **K. Maki**, and **S. Tachibana** (2012). Characterization of complexities in combustion instability in a lean premixed gas-turbine model combustor. *Chaos: An Interdisciplinary Journal of Nonlinear Science*, **22**(4), 043128.

28. **Gotoda, H.**, **H. Nikimoto**, **T. Miyano**, and **S. Tachibana** (2011). Dynamic properties of combustion instability in a lean premixed gas-turbine combustor. *Chaos: An Interdisciplinary Journal of Nonlinear Science*, **21**(1), 013124.

29. **Gotoda, H.**, **Y. Shinoda**, **M. Kobayashi**, **Y. Okuno**, and **S. Tachibana** (2014). Detection and control of combustion instability based on the concept of dynamical system theory. *Physical Review E*, **89**(2), 022910.

30. **Griebel, P.**, **E. Boschek**, and **P. Jansohn** (2007). Lean blowout limits and nox emissions of turbulent, lean premixed, hydrogen-enriched methane/air flames at high pressure. *Journal of engineering for gas turbines and power*, **129**(2), 404–410.

31. **Guethe, F.**, **D. Guyot**, **G. Singla**, **N. Noiray**, and **B. Schuermans** (2012). Chemiluminescence as diagnostic tool in the development of gas turbines. *Applied Physics B*, **107**(3), 619–636.

32. **Higgins, B.** (1802). cited by w. nicholson, on the sound produced by a current of hydrogen gas passing through a tube. with a letter from dr. higgins, respecting the time of its discovery. *J. Nat. Phil., Chem., and the Arts*, **1**, 129–131.

33. **Jacob, R.**, **K. Harikrishnan**, **R. Misra**, and **G. Ambika** (2016). Uniform framework for the recurrence-network analysis of chaotic time series. *Physical Review E*, **93**(1), 012202.

34. **Jahnke, C. C.** and **F. E. Culick** (1994). Application of dynamical systems theory to nonlinear combustion instabilities. *Journal of Propulsion and Power*, **10**(4), 508–517.

35. **Johnson, S.**, *Emergence: The connected lives of ants, brains, cities, and software*. Simon and Schuster, 2002.

36. **Junge, O.** (2012). Estimating long term behavior of flows without trajectory integration: An infinitesimal generator approach.

37. **Juniper, M. P.** and **R. Sujith** (2018). Sensitivity and nonlinearity of thermoacoustic oscillations. *Annual Review of Fluid Mechanics*, **50**(1), 661–689.

38. **Kabiraj, L.**, **A. Saurabh**, **P. Wahi**, and **R. Sujith** (2012). Route to chaos for combustion instability in ducted laminar premixed flames. *Chaos: An Interdisciplinary Journal of Nonlinear Science*, **22**(2), 023129.

39. **Keller, J. .**, **L. Vaneveld**, **D. Korschelt**, **G. Hubbard**, **A. Ghoniem**, **J. Daily**, and **A. Oppenheim** (1982). Mechanism of instabilities in turbulent combustion leading to flashback. *Aiaa Journal*, **20**(2), 254–262.

40. **Lacasa, L.**, **B. Luque**, **F. Ballesteros**, **J. Luque**, and **J. C. Nuno** (2008). From time series to complex networks: The visibility graph. *Proceedings of the National Academy of Sciences*, **105**(13), 4972–4975.

41. **Lesne, A.** and **M. Laguës**, *Scale invariance: From phase transitions to turbulence*. Springer Science & Business Media, 2011.

42. **Lieuwen, T.** (2003). Modeling premixed combustion-acoustic wave interactions: A review. *Journal of propulsion and power*, **19**(5), 765–781.

43. **Lieuwen, T.** and **Y. Neumeier** (2002). Nonlinear pressure-heat release transfer function measurements in a premixed combustor. *Proceedings of the Combustion Institute*, **29**(1), 99–105.

44. **Lieuwen, T.**, **Y. Neumeier**, and **B. Zinn** (1998). The role of unmixedness and chemical kinetics in driving combustion instabilities in lean premixed combustors. *Combustion Science and Technology*, **135**(1-6), 193–211.

45. **Longwell, J. P.**, **E. E. Frost**, and **M. A. Weiss** (1953). Flame stability in bluff body recirculation zones. *Industrial & Engineering Chemistry*, **45**(8), 1629–1633.

46. **Luque, B.**, **L. Lacasa**, **F. Ballesteros**, and **J. Luque** (2009). Horizontal visibility graphs: Exact results for random time series. *Physical Review E*, **80**(4), 046103.

47. **Macquisten, M.** and **A. Dowling** (1993). Low-frequency combustion oscillations in a model afterburner. *Combustion and flame*, **94**(3), 253–264.

48. **Marwan, N.**, **J. F. Donges**, **Y. Zou**, **R. V. Donner**, and **J. Kurths** (2009). Complex network approach for recurrence analysis of time series. *Physics Letters A*, **373**(46), 4246–4254.

49. **Marwan, N.** and **J. Kurths** (2015). Complex network based techniques to identify extreme events and (sudden) transitions in spatio-temporal systems. *Chaos: An Interdisciplinary Journal of Nonlinear Science*, **25**(9), 097609.

50. **Marwan, N.**, **M. C. Romano**, **M. Thiel**, and **J. Kurths** (2007). Recurrence plots for the analysis of complex systems. *Physics reports*, **438**(5), 237–329.

51. **Marwan, N.**, **N. Wessel**, **U. Meyerfeldt**, **A. Schirdewan**, and **J. Kurths** (2002). Recurrence-plot-based measures of complexity and their application to heart-rate-variability data. *Physical review E*, **66**(2), 026702.

52. **McManus, K.**, **T. Poinsot**, and **S. M. Candel** (1993). A review of active control of combustion instabilities. *Progress in energy and combustion science*, **19**(1), 1–29.

53. **Milgram, S.** (1967). The small world problem. *Psychology today*, **2**(1), 60–67.

54. **Mitchell, M.** (2006). Complex systems: Network thinking. *Artificial Intelligence*, **170**(18), 1194–1212.

55. **Mondal, S.**, **S. A. Pawar**, and **R. I. Sujith** (2017). Synchronous behaviour of two interacting oscillatory systems undergoing quasiperiodic route to chaos. *Chaos: An Interdisciplinary Journal of Nonlinear Science*, **27**(10), 103119.

56. **Muruganandam, T.**, **S. Nair**, **D. Scarborough**, **Y. Neumeier**, **J. Jagoda**, **T. Lieuwen**, **J. Seitzman**, and **B. Zinn** (2005). Active control of lean blowout for turbine engine combustors. *Journal of Propulsion and Power*, **21**(5), 807–814.

57. **Muruganandam, T.** and **J. Seitzman** (2012). Fluid mechanics of lean blowout precursors in gas turbine combustors. *International Journal of Spray and Combustion Dynamics*, **4**(1), 29–60.

58. **Murugesan, M.** and **R. Sujith** (2015). Combustion noise is scale-free: transition from scale-free to order at the onset of thermoacoustic instability. *Journal of Fluid Mechanics*, **772**, 225–245.

59. **Murugesan, M.** and **R. Sujith** (2016). Detecting the onset of an impending thermoacoustic instability using complex networks. *Journal of Propulsion and Power*, **32**(1), 707–712.

60. **Nair, S.** and **T. Lieuwen** (2005). Acoustic detection of blowout in premixed flames. *Journal of Propulsion and Power*, **21**(1), 32–39.

61. **Nair, S.** and **T. C. Lieuwen** (2007). Near-blowoff dynamics of a bluff-body stabilized flame. *Journal of Propulsion and power*, **23**(2), 421–427.

62. **Nair, V.** and **R. Sujith** (2013). Identifying homoclinic orbits in the dynamics of intermittent signals through recurrence quantification. *Chaos: An Interdisciplinary Journal of Nonlinear Science*, **23**(3), 033136.

63. **Nair, V.** and **R. Sujith** (2014). Multifractality in combustion noise: predicting an impending combustion instability. *Journal of Fluid Mechanics*, **747**, 635–655.

64. **Nair, V.** and **R. Sujith** (2015). A reduced-order model for the onset of combustion instability: physical mechanisms for intermittency and precursors. *Proceedings of the Combustion Institute*, **35**(3), 3193–3200.

65. **Nair, V.**, **G. Thampi**, **S. Karuppusamy**, **S. Gopalan**, and **R. Sujith** (2013). Loss of chaos in combustion noise as a precursor of impending combustion instability. *International journal of spray and combustion dynamics*, **5**(4), 273–290.

66. **Nair, V.**, **G. Thampi**, and **R. Sujith** (2014). Intermittency route to thermoacoustic instability in turbulent combustors. *Journal of Fluid Mechanics*, **756**, 470–487.

67. **Newman, M. E.** (2003). The structure and function of complex networks. *SIAM review*, **45**(2), 167–256.

68. **Okuno, Y.**, **M. Small**, and **H. Gotoda** (2015). Dynamics of self-excited thermoacoustic instability in a combustion system: Pseudo-periodic and high-dimensional nature. *Chaos: An Interdisciplinary Journal of Nonlinear Science*, **25**(4), 043107.

69. **Pawar, S. A.**, **A. Seshadri**, **V. R. Unni**, and **R. I. Sujith** (2017). Thermoacoustic instability as mutual synchronization between the acoustic field of the confinement and turbulent reactive flow. *Journal of Fluid Mechanics*, **827**, 664âĂŞ693.

70. **Poinsot, T. J.**, **A. C. Trouve**, **D. P. Veynante**, **S. M. Candel**, and **E. J. Esposito** (1987). Vortex-driven acoustically coupled combustion instabilities. *Journal of fluid mechanics*, **177**, 265–292.

71. **Rajaram, R.** and **T. Lieuwen** (2009). Acoustic radiation from turbulent premixed flames. *Journal of Fluid Mechanics*, **637**, 357–385.

72. **Rayleigh, J. W. S.** (1878). The explanation of certain acoustical phenomena. *Nature*, **18**(455), 319–321.

73. **Renard, P.-H.**, **D. Thevenin**, **J.-C. Rolon**, and **S. Candel** (2000). Dynamics of flame/vortex interactions. *Progress in energy and combustion science*, **26**(3), 225–282.

74. **Richards, G. A.** and **M. C. Janus**, Characterization of oscillations during premix gas turbine combustion. *In ASME 1997 International Gas Turbine and Aeroengine Congress and Exhibition*. American Society of Mechanical Engineers, 1997.

75. **Rijke, P. L.** (1859). Lxxi. notice of a new method of causing a vibration of the air contained in a tube open at both ends. *The London, Edinburgh, and Dublin Philosophical Magazine and Journal of Science*, **17**(116), 419–422.

76. **Rogers, D. E.** and **F. E. Marble** (1956). A mechanism for high frequency oscillations in ramjet combustors and afterburners. *Jet Propulsion*, **26**(1), 456–462.

77. **Romano, M. C.**, **M. Thiel**, **J. Kurths**, **I. Z. Kiss**, and **J. Hudson** (2005). Detection of synchronization for non-phase-coherent and non-stationary data. *EPL (Europhysics Letters)*, **71**(3), 466.

78. **Romano, M. C.**, **M. Thiel**, **J. Kurths**, and **W. von Bloh** (2004). Multivariate recurrence plots. *Physics letters A*, **330**(3-4), 214–223.

79. **Sampath, R.** and **S. R. Chakravarthy** (2016). Investigation of intermittent oscillations in a premixed dump combustor using time-resolved particle image velocimetry. *Combustion and Flame*, **172**, 309–325.

80. **Schadow, K.** and **E. Gutmark** (1992). Combustion instability related to vortex shedding in dump combustors and their passive control. *Progress in Energy and Combustion Science*, **18**(2), 117–132.

81. **Schäfer, C.**, **M. G. Rosenblum**, **H.-H. Abel**, and **J. Kurths** (1999). Synchronization in the human cardiorespiratory system. *Physical Review E*, **60**(1), 857.

82. **Schefer, R.**, Combustion of hydrogen-enriched methane in a lean premixed swirl burner. *In Proceedings of the 2001 DOE hydrogen program review*. 2001.

83. **Seshadri, A.**, **V. Nair**, and **R. Sujith** (2016). A reduced-order deterministic model describing an intermittency route to combustion instability. *Combustion Theory and Modelling*, **20**(3), 441–456.

84. **Shanbhogue, S. J.**, **S. Husain**, and **T. Lieuwen** (2009). Lean blowoff of bluff body stabilized flames: Scaling and dynamics. *Progress in Energy and Combustion Science*, **35**(1), 98–120.

85. **Shivashankara, B.**, **W. Strahle**, and **J. Handley**, Combustion noise radiation by open turbulent flames. *In Aeroacoustics Conference*. 1973.

86. **Sivakumar, R.** and **S. Chakravarthy** (2008). Experimental investigation of the acoustic field in a bluff-body combustor. *International Journal of Aeroacoustics*, **7**(3-4), 267–299.

87. **Smith, D. A.** and **E. E. Zukoski** (1985). Combustion instability sustained by unsteady vortex combustion.

88. **Sondhauss, C.** (1850). Über die schallschwingungen der luft in erhitzten glasröhren und in gedeckten pfeifen von ungleicher weite. *Annalen der Physik*, **155**(1), 1–34.

89. **Spalding, D. B.**, *Some fundamentals of combustion*, volume 2. Academic Press, 1955.

90. **Strahle, W. C.** (1977). Combustion noise.

91. **Strahle, W. C.** and **J. I. Jagoda**, Fractal geometry applications in turbulent combustion data analysis. *In Symposium (International) on Combustion*, volume 22. Elsevier, 1989.

92. **Strozzi, F.**, **J.-M. Zaldívar**, **K. Poljanšek**, **F. Bono**, and **E. Gutierrez**, *From complex networks to time series analysis and viceversa: Application to metabolic networks*. Citeseer, 2009.

93. **Sujith, R.**, **G. Waldherr**, **J. Jagoda**, and **B. Zinn** (2000). Experimental investigation of the evaporation of droplets in axial acoustic fields. *Journal of Propulsion and Power*, **16**(2), 278–285.

94. **Takens, F.** (1981). Lecture notes in mathematics. *by DA Rand and L.-S. Young Springer, Berlin*, **898**, 366.

95. **Thampi, G.** and **R. Sujith** (2015). Intermittent burst oscillations: Signature prior to flame blowout in a turbulent swirl-stabilized combustor. *Journal of Propulsion and Power*, **31**(6), 1661–1671.

96. **Thiruchengode, M.** (2006). *Sensing and dynamics of lean blowout in a swirl dump combustor*. Ph.D. thesis, Georgia Institute of Technology.

97. **Tony, J.**, **E. Gopalakrishnan**, **E. Sreelekha**, and **R. Sujith** (2015). Detecting deterministic nature of pressure measurements from a turbulent combustor. *Physical Review E*, **92**(6), 062902.

98. **Unni, V. R.**, **A. Mukhopadhyay**, and **R. Sujith** (2015). Online detection of impending instability in a combustion system using tools from symbolic time series analysis. *International Journal of Spray and Combustion Dynamics*, **7**(3), 243–255.

99. **Unni, V. R.** and **R. Sujith** (2015). Multifractal characteristics of combustor dynamics close to lean blowout. *Journal of Fluid Mechanics*, **784**, 30–50.

100. **Unni, V. R.** and **R. Sujith** (2017). Flame dynamics during intermittency in a turbulent combustor. *Proceedings of the Combustion Institute*, **36**(3), 3791–3798.

101. **Venkataraman, K.**, **L. Preston**, **D. Simons**, **B. Lee**, **J. Lee**, and **D. Santavicca** (1999). Mechanism of combustion instability in a lean premixed dump combustor. *Journal of Propulsion and Power*, **15**(6), 909–918.

102. **Watts, D. J.** and **S. H. Strogatz** (1998). Collective dynamics of âĂŸsmall-worldâĂŹnetworks. *nature*, **393**(6684), 440.

103. **Webber, C. L.** and **J. P. Zbilut** (1994). Dynamical assessment of physiological systems and states using recurrence plot strategies. *Journal of applied physiology*, **76**(2), 965–973.

104. **Xu, X.**, **J. Zhang**, and **M. Small** (2008). Superfamily phenomena and motifs of networks induced from time series. *Proceedings of the National Academy of Sciences*, **105**(50), 19601–19605.

105. **Yu, M. H.** and **P. A. Monkewitz** (1990). The effect of nonuniform density on the absolute instability of two-dimensional inertial jets and wakes. *Physics of Fluids A: Fluid Dynamics*, **2**(7), 1175–1181.

106. **Zhang, J.** and **M. Small** (2006). Complex network from pseudoperiodic time series: Topology versus dynamics. *Physical review letters*, **96**(23), 238701.

107. **Zinn, B. T.** and **T. C. Lieuwen** (2005). Combustion instabilities: Basic concepts. *Combustion Instabilities in Gas Turbine Engines: Operational Experience, Fundamental Mechanisms, and Modeling*, **210**, 3–26.

108. **Zukoski, E. E.** (1955). The role of wake transition in the process of flame stabilization on bluff bodies. *Combustion Researches and Reviews*.

LIST OF PAPERS BASED ON PROJECT WORK

REFEREED JOURNALS

1. **V. Godavarthi**, S. A. Pawar, V. R. Unni, R. I. Sujith, N. Marwan and Jürgen Kurths (2018) Coupled interaction between unsteady flame dynamics and acoustic field in a turbulent combustor. *Chaos: An Interdisciplinary Journal of Nonlinear Science*, **28**, 113111.

2. **V. Godavarthi**, V. R. Unni, E. A. Gopalakrishnan, R. I. Sujith (2017) Recurrence networks to study dynamical transitions in a turbulent combustor. *Chaos: An Interdisciplinary Journal of Nonlinear Science*, **27(6)**, 063113.

POSTER PRESENTATION

V. Godavarthi, S. A. Pawar, V. R. Unni, R. I. Sujith, N. Marwan and Jürgen Kurths (2018) Analyzing synchronization transition to thermoacoustic instability using recurrences in phase space. *Conference on Nonlinear Systems and Dynamics*, New Delhi, 2018.